In vitro study of a selective PI3K inhibitor on brain metastases

Emma Rigg

This thesis is submitted in partial fulfilment of the requirements for the degree of Master in Medical Biology - Biomedicine

The Faculty of Medicine and Dentistry - Department of Biomedicine

University of Bergen

Spring 2020

Acknowledgements

First and foremost, I would like to express my gratitude to Professor Frits Thorsen for his guidance and support throughout this project, from directing me with my experiments to his help with discussion and editing while writing my thesis.

My thanks to all the core facility personnel who helped me with instrumental experiments. Thanks to Endy Spriet for help with the Incucyte and Nikon microscope and the perfect scratches for my scratch wound assays, and to Magdalena Keindl for introducing me to flow cytometry and helping me set up my experiments.

To all those in the Translational Cancer Research group who helped me throughout the year, thank you so much for all your help. Thank you to the technicians for their constant support in the lab, Halala for always being around whenever there were any issues in the lab, and Marzieh for always saving me some food from the break room.

I want to extend my gratitude for all those in the Brain Metastasis Research lab. Tuyen for your absolutely endless support in cell culture, western blotting and through happily helping me out every morning when I'd come to you with questions. Erlend, Tobias and Yulin for being around for discussions both in and out of lab meetings, and Trond Are for helping me out in the beginning with my viability assay analyses.

Sayintha, I couldn't have gotten through this without our de-stressing tea breaks on long days of experiments, well-needed dinners with you and Dayne and the constant motivation working beside you both in the lab and in the office. Christina and Agathe, through your busy schedules, the conversations we had whenever managing to be in the office together helped get me through. Thank you Andreas for the lunchtimes where you trekked over from BUS just to hang with me. Ole, your daily and immeasurable support throughout the duration of this thesis was truly critical in my journey throughout the year and I am so grateful.

My sincerest love to all the friends I've made in Bergen. To my family, parents in Canada and brothers in Japan, thank you for the unconditional love and encouragement you've sent from afar.

Bergen, May 2020

Emma Rigg

Table of Contents

List of Abbreviations

Abbreviation	Full Name
Av	Annexin V
BAD	BCL2 associated agonist of cell death
BBB	Blood-brain barrier
BCC	Basal cell carcinoma
BRAF	B-Raf proto-oncogene, a serine/threonine kinase
CDKN2A	Cyclin-dependent kinase inhibitor 2A
CNS	Central nervous system
CREB	cAMP response element-binding protein
CTLA-4	Cytotoxic T-lymphocyte-associated protein 4
DNA	Deoxyribonucleic acid
EGFR	Epidermal growth factor receptor
EMT	Epithelial–mesenchymal transition
ERK	Extracellular signal-regulated kinases
FDA	Food and Drug Administration
FGFR2	Fibroblast Growth Factor Receptor 2
FOXO	Forkhead box O
G_2/M	G_2-M DNA damage checkpoint
GAPDH	Glyceraldehyde-3-Phosphate Dehydrogenase
GDP	Guanosine diphosphate
GTP	Guanosine-5'-triphosphate
HER2	Human epidermal growth factor receptor 2
MAPK	Mitogen-activated protein kinase
MEK	Mitogen-activated protein kinase kinase
MRI	Magnetic resonance imaging
mTOR	Mammalian target of rapamycin
mTORC1	Mammalian target of rapamycin complex 1
mTORC2	Mammalian target of rapamycin complex 2
NF1	Neurofibromin 1
NMSC	Nonmelanoma skin cancer
p14ARF	ARF tumor suppressor

p53	Tumor protein p53
PARP	Poly(ADP)-ribose polymerase
PD-1	Programmed cell death protein 1
PDGFRB	Platelet-derived growth factor receptor beta
PET/CT	Positron emission tomography-computed tomography
PI	Propidium iodide
PI3K	Phosphoinositide 3-kinase
PI3Kα	Phosphoinositide 3-kinase alpha
PIK3CA	Phosphatidylinositol-4,5-bisphosphate 3-kinase, catalytic subunit alpha
PIK3CB	Phosphatidylinositol-4,5-bisphosphate 3-kinase, catalytic subunit beta
PIP_2	Phosphatidylinositol 4,5-bisphosphate
PIP_3	Phosphatidylinositol (3,4,5)-trisphosphate
PTEN	Phosphatase and tensin homolog
PUVA	Psoralen and ultraviolet A
RAF	Rapidly accelerated fibrosarcoma protein
ROS	Radical oxygen species
RTK	Receptor tyrosine kinase
SCC	Squamous cell carcinoma
SRS	Stereotactic Radiosurgery
TGF-β	Transforming growth factor beta
TNM	Tumour-node-metastasis
TSC1/2	Tuberous sclerosis complex 1/2
TUNEL	Terminal deoxynucleotidyl transferase dUTP nick end labeling
UVR	Ultraviolet radiation
VEGF	Vascular endothelial growth factor
WBRT	Whole brain radiotherapy
WHO	World Health Organization

Summary

Melanoma incidence rates in Norway have increased 8-fold in the last decades, resulting in the highest mortality rates in Europe. Malignant melanoma is an extremely aggressive skin cancer and has the highest propensity of all cancers to metastasize to the brain. Melanoma patients with brain metastases have a very poor prognosis, and even with medical treatment the average survival time after diagnosis is around 4 months. The presence of the blood brain barrier limits around 98% of chemotherapeutic drugs from entering the brain and targeted therapies often lead to development of acquired resistance after a few months.

Melanoma has the highest mutation rates of all malignant tumours, often resulting in the dysregulation of the MAPK and PI3K signaling pathways, that promote survival and proliferation of tumour cells. PI3K is a phosphatidylinositol 3-kinase that initiates the downstream signaling in response to a receptor tyrosine kinase activation and is currently being targeted to inhibit tumour growth. It has four major isoforms, with PI3Kα being the most active in melanoma. HS-173 is an extremely potent PI3Kα inhibitor that has been shown to inhibit tumour growth in several cancers at low doses, regardless of mutational status. The main aim of this thesis was to evaluate the effect of an isoform-specific PI3Kα inhibitor on four human brain metastatic melanoma cell lines *in vitro*.

HS-173 showed a dose-dependent inhibition of cell viability for all four cell lines in monolayer cultures, all with IC_{50} doses below 1 µM. Microscopy revealed that HS-173 induced a rounded morphological change after treatment. HS-173 also reduced migration and proliferation in all the cell lines as shown by a wound healing assay. Through flow cytometric analysis, we found that apoptosis was induced by the drug. Western blotting revealed that HS-173-induced inhibition of PI3Kα downregulated the activation of downstream effectors, in particular the phosphorylation of Akt in all four cell lines. Also, some inhibition of mTOR and PI3Kα expression levels was seen.

In conclusion, we found that HS-173 is an effective inhibitor of melanoma brain metastases *in vitro,* through inhibition of cell growth, migration and viability, induction of apoptosis and reduction of PI3K pathway signaling.

1.0 Introduction

1.1 What is Skin Cancer?

Skin cancer is one of the most widespread malignancies in the world and is commonly separated into two categories: non-melanoma skin cancers (NMSC) and malignant melanoma. NMSCs comprise 99% of all skin cancers, with the majority of cases consisting of basal cell carcinoma (BCC) and squamous cell carcinoma (SCC)[1]. While BCC and SCC make up the majority of all skin cancer incidences, with rates 18-20 times higher than that of melanoma**,** the actual statistics for these cancers are quite unreliable as NMSCs are not necessarily reported to national cancer registries[2]. Both cancers have low mortality rates so vigilant reporting is uncommon, with metastases found in up to 0.05% of cases of BCC and 1.2% of cases of SCC[2,3]. BCC affects the basal cells of the epidermis, and SCC is found in squamous cells (**Fig. 1.1)**[4].

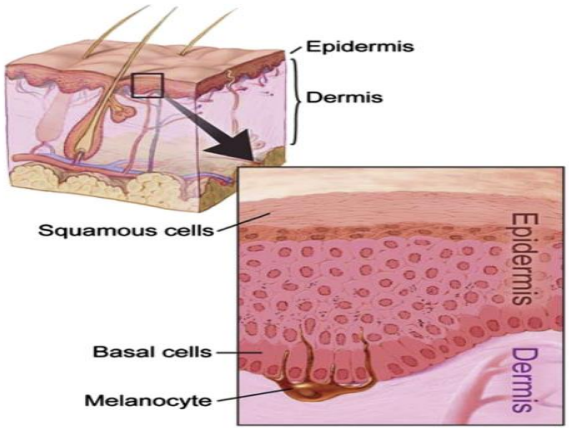

Figure 1.1: Composition of normal layers of the skin: Illustration depicting the upper layers of the skin including major cells and locations within the tissue layers. Figure from The National Cancer Institute. Image taken from Bliss 2005.

The final 1% of skin cancer incidence is attributed to melanoma, a cancer of the melanocytes in the epidermal layer of the skin. Melanocytes, found in the stratum corneum layer of the epidermis, alongside the basal cells, contain melanin that helps to protect the body from UV radiation-induced damage. Although melanoma cases make up less than 1% of all skin cancer cases, they account for the majority of skin cancer deaths (75%), and almost 1% of total cancer-related deaths[5]**.**

1.1.1 Epidemiology, Incidence, and Survival

Melanoma is the 19th most common cancer diagnosed in both women and men, with Norway having the 3rd highest incidence rate in the world and the highest in Europe, with 29.6

cases per 100 000 people[6]**.** Since 1952, the incidence rate has increased eightfold across Norway[7]. According to the WHO Globocan 2018 world statistics of cancer, melanoma of the skin is the 5th most common form of cancer in Norway, and the 7th leading cause of cancer-related deaths[6]. Women have a slightly higher rate of incidence than men, at 30.7 per 100 000 compared to 29.0 per 100 000 respectively[6]. However, there is some evidence that over the age of 70, incidence in men is higher than in women. It has been speculated that the rates of melanoma are linked to socioeconomic status, as people with higher living standards can afford to go on vacation to sunny places or tan in solariums. Additionally, due to the lack of sun in Norway, it has been suggested that Norwegians tend to have more unhealthy tanning habits when there is sun available[8,9].

Men are more likely to be diagnosed on their trunk and back, while women have more cases on their lower extremities including legs and feet[10]. White non-Hispanic populations are the most at risk of all races[11] and the geography of incidence reflects the racial stratification of melanoma. The highest rates are found in countries with large non-Hispanic Caucasian populations exposed to high UV such as New Zealand and Australia (35.8 and 35.1 per 100 000 respectively)[12].

Survival rates for melanoma vary widely, primarily according to the race of the patient and staging of the disease. Mortality rates have been gradually increasing over the last several decades in areas with high incidences, such as Australia, New Zealand, as well as Norway and Sweden. Interestingly, in the United States the 5-year survival rate (normalized to all stages) remains at around 94% for non-Hispanic Whites, however African American rates are much lower at around 64%[5]**.** This variation has been attributed to socioeconomic reasons, as those with higher status have more medical access, insurance and education to aid in early diagnosis[11,13]. In 2012, the cutaneous melanoma mortality rate in Norway was also the highest in Europe and third in the world. On average, Norwegians have a more advanced staged melanoma at diagnosis, possibly due to a lack of awareness, which increases the risk of mortality[14]. It is important to note that these survival rates are overall averages, although the melanoma survival rate varies widely between stages and grades. This will be further described in **Section 1.5**.

1.2 Causes and Risk Factors of Melanoma

Melanoma is considered a multifactorial cancer, due to the variety of risk factors that can lead to it. The risk factors for melanoma can be categorized into endogenous and exogenous

factors. Exogenous risk factors are external or environmental factors that are often mediated through lifestyle such as sun exposure. Endogenous risk factors are less modifiable and related to the inherent characteristics of a patient, such as DNA repair mechanisms or race[15].

The major environmental risk factor for melanoma, as well for the other skin cancers, is ultraviolet radiation (UVR) exposure. UVR has two wavelengths relevant for skin cancer, UVA and UVB. UVA can induce degenerative tissue damage deep in the skin, while UVB is the primary cause of sunburns and directly damages DNA through the formation of pyrimidine dimers[16]. Although there is some variance between cumulative and chronic sun exposure, there may be a correlation between melanoma and unaccustomed sun exposure, i.e. pale-skinned people and acute sunburns, which may explain why the rates are so high in countries with pale-skinned populations and less sun (i.e. Norway and Sweden)[17]. Interestingly**,** chronic UV exposure is more correlated with non-melanoma skin cancers, although the reason behind this is not entirely understood[18]. A meta-analysis of UV light exposure and skin cancer found that the use of tanning beds before the age of 35 and childhood sunburns increase the risk of melanoma later in life, and that the highest risk group in Norway was women who used tanning equipment at least once a month between the ages of 20 and 29[19]. It has also been suggested that psoralen and ultraviolet A (PUVA), a treatment for psoriasis, has a dose-dependent increase in risk of melanoma in patients with pale, burn-susceptible skin[20]. Additionally, geographic location can also increase the risk, as the strength of UV rays along the equator is much stronger than in Northern Europe, giving some explaining to why melanoma rates are some of the highest in Australia and New Zealand[6]. It is speculated that ozone layer holes are allowing more UVB into our environment, and although there are no recent articles suggesting a causal effect, there are many studies predicting increased risk as ozone depletion worsens[21-23].

Other less common environmental factors include some photosensitive drugs that upon UVR exposure can lead to radical oxygen species (ROS) formation, and some cosmetic ingredients such as para-aminophenol and para-phenylenediamine which have carcinogenic properties when exposed to skin[24].

One endogenous risk factor of melanoma is race, as skin type is often denoted by genetics within races. The risk of developing malignant melanoma is 1 in 40 for non-Hispanic Caucasians, 1 in 1000 for Blacks and 1 in 200 for Latin Americans[25]. Different skin types within Caucasians also affect the individual risk, with type 1 and 2 having the highest risk when exposed to UVR out of the six skin types shown in **Fig. 1.2**. Higher risk of sunburn correlates

with higher melanoma risk as the UV-derived DNA damage from sunburns directly increases the chance of malignant tumour formation[25].

Figure 1.2. Fitzpatrick Sun-Exposed Skin Types: Type I: always reddens, rarely tans. Type II: often reddens and rarely tans. Type III: sometimes reddens and gradually tans. Type IV and V: rarely redden and often tan. Type VI: Never reddens. Taken from Orthaber, 2017.

Another endogenous risk factor of melanoma is melanocytic naevi, colloquially known as moles. A meta-analysis found that the risk factor for people with 101-120 naevi was seven times higher than for those with less than 15 naevi, and people with at least 5 atypical naevi had five times higher incidence of melanoma than those with less than 5 naevi[26]. Atypical is defined as three of the following: poorly defined border, >5mm, varying colours, redness, and asymmetrical[27]. It was also found that up to ¾ of melanoma patients had previously reported their naevi to their doctor and in 25-50% of those it was shown that their tumour was associated with a naevi. Finally, naevi can also be formed through exposure to sunlight and the number alone can be an indication of UV exposure[26].

It has been indicated that melanoma can be familial. Inherited melanoma is typically found in patients under 40 years, usually with multiple cases within one side of the family[28]. It is thought to be linked to a mutation in a gene important in the cell cycle pathway: cyclin-dependent kinase inhibitor 2A (*CDKN2A*). *CDKN2A* encodes p16 and p14ARF which are negative regulators of cell proliferation, and have inactivating mutations in up to 40% of melanoma-prone families (3 or more cases of melanoma), but only in 8-15% of overall cases[29,30].

1.3 Biological Aspects of Melanoma

Melanoma is a malignant neoplasm from melanocytes. Melanocytes are neural crest-derived cells, the majority of which are found in the epidermis including skin and eye, but they can also found in other locations such as the nasal cavity and inner ear[31]. The majority of melanomas are found on the skin, and the most common forms of melanoma are cutaneous melanomas, which are comprised of the following sub-groups from most to least common: superficial spreading, nodular, lentigo maligna, and acral lentiginous[18]. Melanoma can be derived from the meninges in the eyes and various mucosal tissues, with rarer forms arising in these areas which include mucosal lentiginous, intraocular, or desmoplastic melanoma[5,18,32].

Primarily, melanocytes are found in the epidermal-dermal junction and produce melanin, a pigmented biopolymer that darkens the skin and protects it from UVR. Skin colour is determined by the amount and distribution of melanocytes within the skin[33]. There are two forms of mammalian melanin, brown-black eumelanin and yellow-red pheomelanin[31]. Melanocytes produce melanin through a lysosome-like structure called a melanosome which is then shuttled to keratinocytes to protect the cells from UVR damage. Melanin functions as a UV-shielding molecule (specifically eumelanin) by scattering UVB photons to prevent the penetration of UV into the epidermis[34]. It has been estimated that melanin absorbs around 50-75% of UVR. Melanin can also act as a free radical mediator to help minimize damage through ROS[35].

1.4 Molecular Aspects of Melanoma

Melanoma is genetically heterogeneous, primarily because the main risk factor (UV radiation) can cause random mutations in the genome. It was recently found through whole-genome sequencing that melanoma is the most highly mutated tumour out of all cancers studied (**Fig. 1.3**)[36].

A driver mutation is a mutation within a cell which gives a selected advantage in its microenvironment, such as increased survival or proliferative capacity. These may be either within a tumour suppressor gene or a proto-oncogene. A tumour suppressor gene is a gene that regulates cell division and replication, and when the tumour suppression gene (such as *CDK2NA*) is mutated, it results in loss or reduction of its function, leading to uncontrolled cell growth. A proto-oncogene is a normal gene that contributes to cell growth, and when mutated (then called an oncogene) leads to overstimulation of the growth or survival pathways. These driver mutations promote genetic instability, which results in additional mutations, perpetuating uncontrolled cell growth.

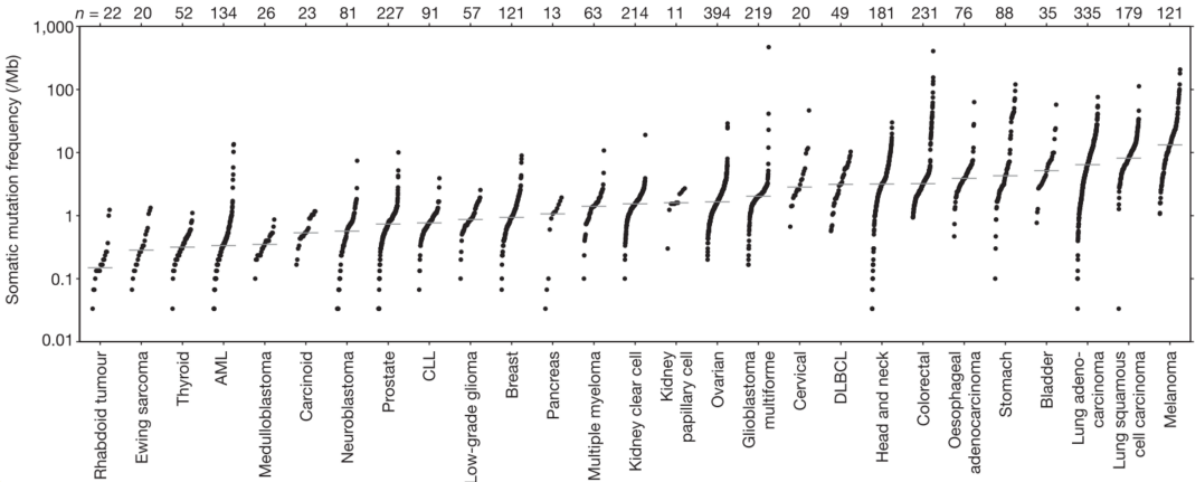

Figure 1.3: Somatic mutation frequencies observed across several types of cancer. Each dot corresponds to a tumour compared to a normal tissue sample, with the vertical position representing totally frequency of somatic mutations in that tumour. Ordered by median mutation frequency from lowest (left) to highest (right). Taken from Lawrence (2013).

The two most important signaling pathways found to be affected by mutations are the mitogen-activated protein kinase (MAPK) pathway and the phospho-inositide-3 (PI3K) pathway[37], which both are involved in cell growth, survival, and proliferation.

In melanoma, mutations in the *BRAF* gene in the MAPK pathway are the most prevalent, and are present in approximately 50% of cases[38-40]. The RAF family of proteins is comprised of signal transduction protein kinases, activated by the RAS family of G-proteins, that play a major role in the MAPK/ERK pathway to help mediate the cell response to growth factor signaling[41,42]. BRAF is highly regulated, efficiently activated by RAS and has a higher basal activity than the other RAFs such as CRAF and ARAF[42,43]. *BRAF* is mutated in several other cancers in addition to melanoma, including cancers in the lung, breast, and liver[44]. In melanoma, 97% of *BRAF* mutations are found in codon 600 of the gene, which corresponds to the active phosphorylation site of the protein. Of these 97%, 90% are comprised of a valine (V) to glutamic acid (E) (V600E) substitution[45]. This mutation constituently activates the protein and induces resistance to feedback mechanisms, leading to increased cell proliferation[46]. It is also worth noting that *BRAF*-mutated tumours seem to have an increased propensity to metastasize to the brain[47,48].

The second most prevalent mutation in melanoma is found in the *NRAS* gene, also in the MAPK pathway. RAS proteins belong to a family of small GTPases that transduce growth signals through the binding of GTP and subsequent activation of downstream effectors, such as RAF. *RAS* gene mutations are the most commonly found alterations in all human cancers, in around 30% of all tumours[49]. In melanoma, activating *NRAS* mutations have been discovered

in 15-30% of cases[38,40,50]. There are three codon 'hotspots' in which 98% of the mutations exist across all *RAS* isoforms: Q61, G12, and G13[51]. These mutations all increase the GTPase activity by favouring the GTP-bound active RAS protein[52,53], and 20-fold more tumours harbour the Q61 arginine (Q61R) mutation, compared to G12 or G13[54,55]. *BRAF* and *NRAS* mutations have been found together, however the mutations are generally mutually exclusive[50,56].

Inactivating mutations in the tumour suppressor gene Neurofibromin 1 (*NF1*) have been discovered in approximately 15% of all cutaneous melanomas[40], and are present in 50% of *BRAF*/*NRAS* wild-type tumours[57,58]. *NF1* is a negative regulator of the MAPK pathway as a GTPase-activating protein to increase the hydrolysis of RAS-bound GTP to result in the inactive GDP-bound RAS[59].

In addition to mutations in the MAPK pathway, the closely associated PI3K pathway is often upregulated. The most common mutation found here is an inactivation of the tumour suppressor gene *PTEN*[39]. The PTEN protein dephosphorylates phosphatidylinositol (3,4,5)-trisphosphate to phosphatidylinositol (4,5)-bisphosphate to prevent downstream Akt activation[60]. PTEN is inactivated in around 10% of primary melanomas, and is frequently associated with BRAF-mutant melanomas, thus causing upregulation in both the PI3K and the MAPK pathways[58,61].

The final major mutation present in melanoma is in the gene *TP53*, which codes for the protein p53, a regulatory protein involved in DNA repair and apoptosis[62]. *TP53* is one of the most commonly mutated proteins across all types of cancer, and it is approximated to be mutated in 36.1% of total cancers[63]. TP53 is mutated in 15-19% of all melanomas, and it is more often in combination with *BRAF* (10%), *RAS* (20%) and *NF1* (30%) mutated cancers than triple wild-type, meaning those without any *BRAF, RAS* or *NF1* mutations [50,58,64]. TP53 is a tumour suppressor gene and therefore has an inactivating mutation that prevents initiation of apoptosis and further enables instability of the genome[62].

1.5 Grading and Staging of Melanoma

There are two key systems for classifying cancer, grading and staging. Grading describes the morphology of the cells within the tumour and the extent of abnormality, whereas

staging describes the size of the primary tumour and the extent of the spread. A general tumour grading system used for melanoma is shown in Table 1.1 below[65]:

Table 1.1 Description of grading system utilized to classify cancer cell abnormality.

Grading	Description
G1	Well differentiated, look like normal cells. Low grade.
G2	Moderately differentiated, look partially abnormal. Moderate grade.
G3	Poorly differentiated and are abnormal. High grade.
G4	Undifferentiated, extremely abnormal. High grade.

65

The staging of melanoma utilizes a tumour-node-metastasis (TNM) system which considers the thickness (mm), number of metastatic nodes, and distant metastases of the tumours. The most recent version of melanoma staging by the American Joint Committee on Cancer considers many more factors for sub-staging, including level of invasion, mitotic rates, and ulceration, however the general staging classifications are found in **Table 1.2** below[5,66,67].

Table 1.2 Description of melanoma staging and correlating survival rates.

	Description	5-Year Survival
Stage 0	Melanoma *in situ*. Abnormal neoplasm confined to epidermis.	-
Stage I	Melanoma confined to the skin. Thickness of <1 mm^2. Can be ulcerated (skin covering is broken open) or not.	92-97%.
Stage II	Melanoma is ulcerated, but not spreading. Thickness is from 1.01 mm to 4.0 mm.	53-81%.
Stage III	Melanoma has metastasized to either one or more lymph nodes, or nearby skin.	40-78%.
Stage IV	Melanoma has spread to internal organs, distant lymph nodes, or distant skin.	15-20%.

5,67,68

1.6 Cancer Metastasis

Metastasis is the process where cancer cells breaks off from the primary tumour, travel through the blood or lymphatic system, and form tumours in secondary organs. Metastases can lead to organ failure, and are responsible for 90% of all cancer deaths[68]. Melanoma has a high propensity to metastasize, and approximately 30% of melanoma patients already have metastatic disease upon presentation[69]. The process of primary tumour cells forming secondary malignancies is known as 'the metastatic cascade' and follows a series of steps that are generally consistent among all cancers: invasion of local tissues, followed by intravasation into lymphatic or blood system, extravasation out of the lymphatic or blood vessels into distant sites, and finally formation of micrometastases and solid tumours[70].

For local invasion, tumour cells must exit the local tissues and enter the stroma, generally through the basement membrane of the tissues. This stage relies on an important process called epithelial to mesenchymal transition (EMT), where cells remodel themselves to a cell type that has improved migration and invasive properties. This transition involves the alteration of cell adhesion proteins (such as integrins and cadherins), loss of cell polarity, and remodelling of the cytoskeleton. This transition is commonly mediated by hypoxia, cytokines, or growth factor release[71].

Once local tissues have been invaded, tumours must enter the local circulatory system to travel throughout the body. Primary tumours often form networks of their own vasculature, which increases the rate of intravasation. Release of VEGF, which can promote vessel leakiness, and matrix metalloproteinase enzymes further help entry of tumour cells into vasculature[72].

A key factor of the metastatic cascade is survival within the circulatory system. This process is stressful to the tumour cells as adhesion-signaling systems are no long available, and they are vulnerable to the immune system and general shear forces[73]. At the site of potential metastasis, there are two possible ways that cells are arrested to start invading those tissues. The first is the possibility that the tumour cells are mechanically trapped within the microvasculature and can no longer move through the vessels, and therefore penetrate through the vessels of the secondary organ (i.e. extravasate) and start growing a tumour at that site[70]. The second is a hypothesis that suggests that certain tumour cells have a tropism to other tissue and this causes a 'homing' of the cells to certain organs.

Extravasation of tumour cells is a similar process to intravasation, in which growth factors and degradative enzymes break down vessel walls and invade the site of metastasis. Formation of vasculature within the metastases is not uncommon, and VEGF plays a key role in this process in melanoma[56].

1.6.1 Melanoma Brain Metastasis and the Blood-Brain Barrier (BBB)

Brain metastases are the most common form of malignancy in the brain, and one of the most devastating complications of cancer. It is estimated that over 100 000 patients develop brain metastases in the United States each year and according to autopsy reports, approximately 25% of patients who die of cancer have brain metastases[74,75]. Incidence rates are increasing, due to improved diagnostics and better treatments of systemic disease[76]. Although all cancer types can metastasize to the brain, lung cancer, breast cancer, and melanoma constitute the majority of brain metastases, accounting for 67-80% of cases[77,78]. Of these three, melanoma has the highest propensity to travel to the brain, so although it does not account for the most cases of brain metastases, it is the most likely cancer to develop one.

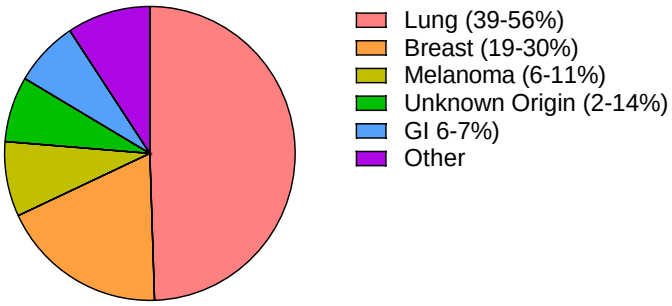

Figure 1.4: Pie chart of the different primary cancers from which brain metastases originate. The chart is based on data published in Nayak, 2011.

It has been estimated that 20-54% of melanoma deaths are due to brain metastases, although autopsy studies show that up to 70% of melanoma patients have brain metastases[79-82]. If untreated, these patients have median survival times ranging from 3-6 months[80,83]. Aggressive treatment (see Chapter 1.7) has prolonged the survival to 12-22 months due to improvement of targeted treatments, depending on the initial prognosis[84,85]. Melanoma patients are more likely to have multiple brain metastases and the majority of these patients will also have metastases to other organs[77,83]. Brain metastases are extremely fatal, as any damage to the central nervous system (CNS) can cause complete shutdown of important bodily functions.

Chemotherapeutic treatment of brain metastases is usually not effective, due to the blood-brain barrier (BBB), which effectively prevents more than 98% of small molecules from entering the brain[86]. The BBB is a highly restrictive barrier between the blood vessels and the brain parenchyma, preventing non-selective transport of molecules through the vasculature. The BBB consists of endothelial cells connected by tight junctions[87]. Pericytes and smooth muscle cells rest on a tight basement membrane around the vasculature, and microglia act as local immune cells, in addition to circulatory immune cells, which may enter brain tissues under certain neurological conditions[88]. Astrocytic end feet surround the endothelial tubes to provide structural integrity and act as a cellular link between the neurons and blood vessels[87]. This restrictive barrier to the brain only allows penetration of molecules less than around 400-500 Da, although hydrophobicity charge and shape of the molecules also play a role[89].

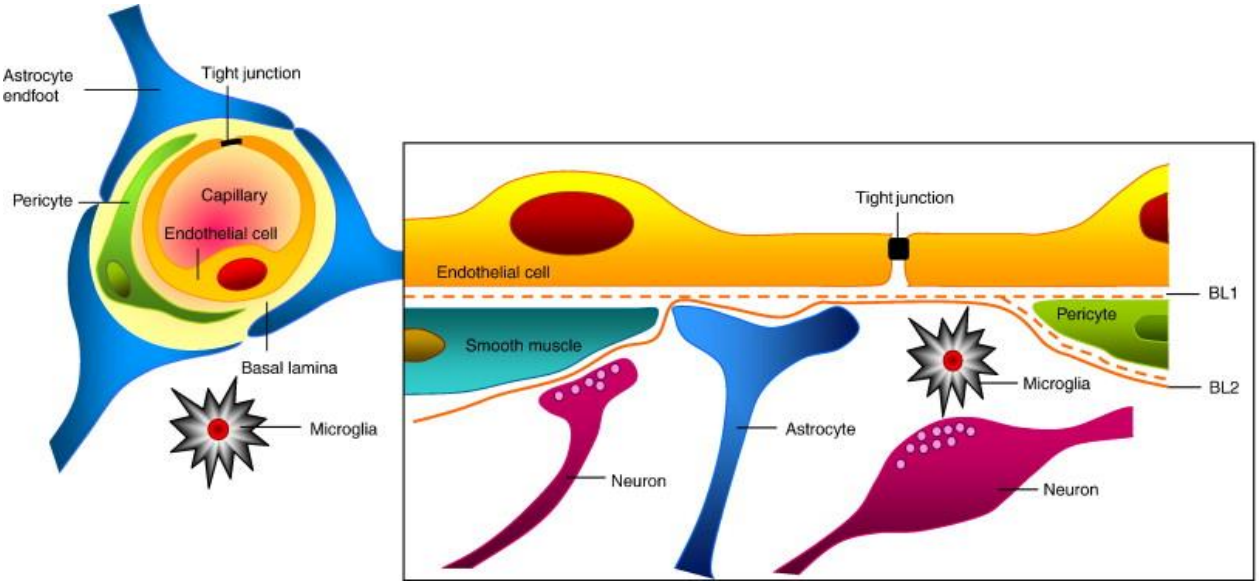

Figure 1.5 Illustration of the blood-brain barrier. The endothelial cells only contain tight junctions, allowing no passive diffusion from blood. Smooth muscle and pericytes structurally support the endothelial cells and are surrounded by two layers of basal lamina (BL1 and BL2) to ensure stability and help mediate blood flow. Astrocyte end feet help maintain the barrier and act as a signalling link between the BBB and neurons. Microglia are the resident immune cells. Taken from Abbot (2010).

1.7 Treatment of Melanoma Brain Metastases

Although there are many different treatments offered to patients with melanoma brain metastases, the poor survival rates clearly indicate their lack of effectiveness. Brain metastases are commonly treated with surgery, radiotherapy, radiosurgery, and chemotherapy[90]. Surgical intervention is regularly performed on patients with one or several lesions, if they are localized in accessible areas, and not too close to critical brain structures. Most melanoma patients have multiple lesions at diagnosis, and the most life-threatening metastases are therefore chosen for

operation. Resected tumour material is also used for histologic assessment to determine a more personalized route of treatment[90].

In the past whole brain radiotherapy (WBRT) combined with corticosteroids has been one of the typical initial treatments for brain metastases, either administered alone or after surgery[91]. Corticosteroids are administered only to reduce symptoms, such as edema and seizures, as they do not decrease tumour burden. Long term use of steroids can cause several side effects ranging from moderate such as increased blood sugar, to life threatening such as gastrointestinal ulceration[92]. WBRT also is a very non-targeted treatment and therefore neurocognitive decline is a major side effect, reducing verbal, recall, and fine motor skills[90].

Stereotactic radiosurgery (SRS) has recently emerged as an effective treatment strategy for brain metastases. SRS is a local radiation treatment, delivering focused, single high-dose radiation through gamma or x-ray beams[93]. When compared to WBRT, SRS does not demonstrate a statistically significant difference in overall survival (7.3 months for SRS vs. 7.2 months for WBRT) in patients with up to ten lesions, but it causes much less adverse side effects during and after treatment such as edema and leukoencephalopathy[94]. However, the development of radiation necrosis 7-12 months after treatment is more common in SRS than in WBRT[95]. Radiation necrosis, occurring in 10-25% of SRS-treated patients, includes psychomotoric impairment, seizures, memory loss, and personality changes[96-98].

Immunotherapy is a type of targeted therapy that aims to induce an immune response within the tumour. Ipilimumab is a monoclonal antibody blocking CTLA-4 that causes continuous activation of T-cell targets in tumour cells. These antibodies are not able to cross an intact BBB, but active T-cells can[90]. In a phase II clinical trial of patients with advanced melanoma and brain metastases, a monoclonal antibody blocking CTLA-4 called ipilimumab showed a CNS response rate of 16%, with a median survival of 7.0 months[99]. Pembrolizumab, a monoclonal antibody activating programmed cell death protein 1 (PD-1) on lymphocytes, was used in a phase II trial with asymptomatic melanoma brain metastases patients. There was a 26% response rate and some patients even lived to 24 months, however there were adverse side effects such as controllable seizures and cerebral edemas[100]. While immunotherapy does seem promising, it has been speculated that patients put onto steroids may not respond to the therapy, and intratumoural inflammation within brain tumours could lead to more extensive neurological symptoms[91].

Finally, the most promising advancement in the treatment of melanoma brain metastases is therapies targeting the proteins that cause dysregulation in major growth pathways. As discussed in **Section 1.4**, melanomas often have activating mutations in the MAPK and PI3K pathways**.** Dabrafenib and vemurafenib both target the BRAF protein and in clinical trials, the use of these drugs has resulted in increased survival compared to controls, with a median life expectancy of 8 months and 5.3 months, as well as response rates of 39% and 16%, respectively[101,102]. Despite their initial effectiveness, a major complication of these drugs is the development of resistance after around 6 months of treatment[103]. Melanoma brain tumours have the capacity to activate underlying mechanisms that help confer resistance to these treatments, so combination treatments are also being attempted to inhibit multiple pathways. These mechanisms include changing signaling proteins from BRAF to CRAF or ARAF, activating tyrosine kinase receptors to promote pathways involved in survival, and mutational alterations in other major effector proteins[104]. Targeting both BRAF and MEK proteins with dabrafenib and trametinib or vemurafenib and cobimetinib is currently being evaluated[105-107]. More recently, targeting the PI3K pathway has been of interest, and there is currently an ongoing study evaluating the effectiveness of the pan-PI3K inhibitor buparlisib in patients with brain metastases[108].

Multimodal treatments used to treat the primary cancer have also been tested on brain metastasis patients, including combined targeted therapies and immunotherapies[109-111]. There have been clinical trials evaluating immunotherapy in combination with WBRT or SRS treatment, with varying results from no improvement compared to that of single modality, to significantly increased life expectancy[112-114].

1.8 PI3K

PI3K proteins are a large family of lipid kinases that are divided into three main classes. Class I PI3Ks are the most common form and most involved in cancer. Class I converts phosphatidylinositol 4,5-bisphosphate (PIP_2) into phosphatidylinositol (3,4,5)-trisphosphate (PIP_3) and is activated by receptor tyrosine kinases (RTKs). Class I PI3Ks are heterodimers made up of a regulatory unit that receives the activating stimulation and a catalytic subunit that detaches and has intrinsic enzymatic ability. There are four isoforms of catalytic subunits denoted by their 110 kDa size: p110α, β, δ, and γ. P110α and p110β are constituently produced in all cells, while p110δ and p100γ are found in leukocytes and have little importance in melanoma[115]. Class II PI3Ks consist only of a single enzymatic subunit and preferentially phosphorylate phosphatidylinositol and phosphatidylinositol 4-phosphate, and have some

involvement in clathrin-mediated endocytosis. Class III PI3Ks are structurally similar to Class I, but their substrate is exclusively phosphatidylinositol, and they are involved in protein autophagy[115]. There is a distant Class IV that does not fit into the category of 'true' PI3Ks but includes distantly-related serine/threonine kinases[116].

As mentioned in **Section 1.4**, the PI3K signaling pathway is often upregulated in melanoma. In brief, the PI3K pathway is a cascade of regulatory proteins, both positive and negative, that regulates essential functions such as angiogenesis, metabolism, transcription, protein synthesis, and apoptosis[117]. PI3K is one of the first modulatory proteins in the pathway and is stimulated by an RTK, either directly or through adaptor molecules. PI3K then converts PIP_2 into PIP_3, which allows binding and activating of PDK1 and Akt, and subsequent downstream activation of other effectors such as mTOR[117].

Because of its involvement in so many important regulatory functions, PI3K is of major importance in cancer, and often has mutations in either PI3K itself, PTEN, or an upstream RTK. The major effect in PTEN-deleted cells is overactivation of Akt, whereas in PI3K-mutated cells there are increased interactions with lipid membranes[118]. Most often mutations in cancers are found in the p110α subunit (gene: *PIK3CA*), but there is also evidence of p110β (gene: *PIK3CB*) activation in HER2-amplified breast cancers[119].

1.8.1 PI3K-Selective Inhibitors

In clinical treatment, three major strategies for PI3K pathway inhibition are currently in use: dual PI3K/mTOR inhibition, pan-PI3K inhibition, or isoform-selective inhibition. Promising results after using the pan-PI3K inhibitor buparlisib have been reported in melanoma brain metastases[120,121]. However, pan-PI3K inhibitors have relatively high rates of adverse side effects due to off-target toxicity such as hyperglycaemia, gastrointestinal intolerance, and stomatitis[122-124]. It has been demonstrated that selective inhibitors have improved specificity and reduced toxicity, and therefore a maximal inhibitory dose without severe side effects may be achieved more easily[123,125,126]. These results may provide the opportunity for combination therapies targeting multiple signaling pathways.

There are few FDA-approved selective inhibitors for PI3K isoforms. A Class Iγ inhibitor for lymphoma patients, and only last year a PI3Kα inhibitor alpelisib was approved treatment in breast cancer patients; however, it has been proven to not cross the blood brain barrier, and has excluded patients with brain metastases in some clinical trials[127,128]. There are several clinical trials investigating other isoforms in varying forms of cancers, with only one

focusing on melanoma specifically with PTEN loss[129-132]. The focus is mainly on breast cancer as up to 70% of breast cancers have PI3K activation and 30% have PI3Kα activating mutations[133]. PI3K reactivation is involved in 20% of melanoma patients with resistance to BRAF and MEK inhibitors[134]. PTEN deletion is often found in combination with BRAF mutations, but not combined with NRAS mutations. In cases of melanoma with BRAF activation and PTEN loss, inhibition of BRAF or MEK is less effective than combined inhibition[135]. PI3K pathway inhibitors have been reported to be effective in BRAF-mutant cancer cell lines, even in those without any PI3K pathway abberations[136,137]. They have also been found to be effective in NRAS mutant melanomas, as Ras is a stimulating protein for both MAPK and PI3K pathways. It should be noted that in melanomas with PTEN loss, p110β seems to be the more active isoform, while those with RTK-driven signaling have more reliance on the p110α isoform[137].

1.8.2 HS-173

HS-173 is an extremely potent PI3Ka inhibitor with an IC_{50} dose of 0.8 nM in cell-free assays[138]. The molecular weight is 422.46 Da, and the molecule acts a competitive inhibitor by binding to the ATP-site of PI3K[138]. It has been found to reduce proliferation and angiogenesis, while promoting apoptosis in breast cancer, liver cancer, pancreatic cancer, and melanoma[139-141]. It has been shown that HS-173 inhibits tumour vascularization by decreasing the expression of HIF1a and VEGF under hypoxic conditions. By inhibiting the PI3K pathway, it decreases EMT transition and metastasis to the liver, lung, and lymph nodes by supressing Akt-driven morphology changes that contribute to cell invasiveness[141]. The anti-tumour effect has been shown in both *in vitro* and *in vivo* models, with no body weight loss in mouse models. While decreasing tumour vascularization, HS-173 also helped to increase vascular morphology by reducing leakiness and further tumour invasiveness in xenograft and metastatic models[140]. Finally, HS-173 has been shown to promote radiosensitivity in pancreatic cancer animal models, with the combination of HS-173 and radiation having a synergistic effect. While promoting apoptosis in tumours, the remaining live cells were found to have a G_2/M phase cell cycle arrest, decreasing the cells' ability to repair and synthesize DNA, leading to radiation sensitivity[142]. In a high-throughput study evaluating effective PI3Ka inhibitors for combination therapies, HS-173 was selected as the most effective and specific PI3Ka inhibitor[143]. These effects suggest that HS-173 is a good candidate for evaluating the effectiveness of PI3Ka inhibition in melanoma brain metastasis.

2.0 Aims

The main aim of this Master thesis was to evaluate the *in vitro* effects of the PI3Kα inhibitor HS-173, on four human melanoma brain metastases cell lines.

Six sub-aims were defined for the work in this Master thesis:

1. To evaluate the effect of HS-173 on cell viability in monolayer cultures.
2. To study potential morphological changes induced by HS-173, using light microscopy.
3. To evaluate the effects of HS-173 on cell proliferation and migration, using a scratch wound assay.
4. To investigate potential apoptotic effects after HS-173 exposure, by flow cytometry.
5. To determine the potential effects on PI3K signaling after HS-173 exposure, using western blot.
6. To evaluate the effect of HS-173 on cell viability on tumour cells grown as 3D spheroids in a soft-agar assay.

3.0 Materials and Methods

3.1 Cell Lines

Experiments were conducted with the four following cell lines: H1, H2, H3 and H10. All cell lines were developed in our laboratory from resected tumours of four patients with malignant melanoma brain metastases. Before tumour material collection, informed written consent was obtained from each patient. The BRAF mutation status of these cell lines was investigated by performing massive parallel sequencing of tumour DNA. Our previous results showed that all cell lines contained a BRAF mutation, with H1, H2 and H10 containing a V600E mutation and H3 showed a novel melanoma mutation L577F[121]. The origin of the cell lines was verified through short tandem repeat (STR) fingerprinting before use, and frequently tested for mycoplasma during the thesis work.

3.1.1 General Culture of Cells

Reagents Name	Company
ALT-DMEM	
Dulbecco's Modified Eagle Medium	Sigma-Aldrich Inc., St. Louis, MO, USA
10% heat-inactivated newborn calf serum	Thermo Fischer Scientific, Waltham, MA, USA
5 µg/mL Plasmocin	Invitrogen, Toulouse, France
2% L-glutamine	BioWhittaker, Verviers, Belgium
100 IU/mL penicillin	BioWhittaker, Verviers, Belgium
100 µL/mL streptomycin	BioWhittaker, Verviers, Belgium
1X PBS	
10X Dulbeccos phosphate-buffered saline	Sigma-Aldrich Inc.
Autoclaved MilliQ water	-

All cells were cultured in ALT-DMEM. Cells were kept in T175 culture flasks (Nunc, Roskilde, Denmark) in a standard incubator at 37 °C, 100% humidity and 5% CO_2 .

Cells were trypsinated at 75-80% confluency using 0.25% Trypsin/EDTA (BioWhittaker). Prior to trypsinization, flasks were washed with 8 mL of 1X PBS prior to adding 4 mL of trypsin and placing in the incubator for 2 mins. Trypsin was neutralized using 6 mL of ALT-DMEM and cells were resuspended by pipetting up and down before adding to fresh flasks for counting.

The cells were counted before *in vitro* experiments were performed. 10 µL of cell suspension was added into a sterile 0.5 mL Eppendorf tube (Eppendorf AG, Hamburg,

Germany) and mixed with 10 µL of Trypan blue stain (Life Technologies, OR, US) to stain dead cell nuclei. 10 µL of the solution was then transferred into each side of a cell counting chamber slide (Thermo Fisher, Invitrogen) and inserted into the Countess Automated Cell Counter (Thermo Fisher, Invitrogen). The mean value from two individual counts of live cells/mL was used to calculate the mean number of cells/mL in the cell solution.

All cells were only used for ten passages after thawing, with one passage being considered as one trypsinization.

3.1.2 Thawing and Freezing of Cells

Cells were thawed by hand and immediately pipetted into a T75 cm^2 flask containing 15 mL of pre-warmed culture media and gently resuspended prior to incubation at 37 °C, 5% CO_2 and 100% humidity.

Cells were frozen when a T175 cm^2 flask was 70-80 % confluent. Cells were first passaged as described in **3.1.1**, and the 10 mL cell solution was transferred to a Falcon tube (Thermo Scientific). The cell solution was centrifuged at 900 x *g* for 4 mins, the supernatant was removed, and the cell pellet was resuspended in 4mL of cold freezing medium. The freezing medium was prepared by mixing 1:1 solution of ALT-DMEM + 20% FBS and PBS + 20% DMSO. 1 mL aliquots of cells were frozen in cryotubes (Nunc, Roskilde, Denmark) at -80 °C in a Mr. Frosty Freezing Container (Thermo Scientific, Nalgene) overnight and transferred to a cryotank for long term storage.

3.2. Experimental Preparation

3.2.1 Drug Preparation: HS-173 PI3Kα inhibitor

Table 3.2: Information about the HS-173 inhibitor, taken from the Selleck Chemicals webpage[138].

Synonym:	N/A
Application:	HS-173 is a potent **PI3Kα** inhibitor
CAS Number:	1276110-06-5
Purity:	99.6 %
Molecular weight:	422.46 (Da)
Molecular formula:	$C_{21}H_{18}N_4O_4S$
Appearance:	Powder

Physical state:	Solid
Solubility:	84 mg/mL (198.84 mM) in DMSO, insoluble in water
Storage:	-80 °C

The drug was received as a powder and diluted to a stock solution of 100 mM in DMSO, aliquoted in 30 µL and stored at -80 °C. For experiments, stock solutions were thawed in a 37 °C water bath and diluted in ALT DMEM to the required concentrations.

3.3. Monolayer Viability Assay

The cell lines H1, H2, H3 and H10 were seeded in 96 well plates (Nunc) at a concentration of $5.0x10^3$ cells/100 µL in each well and left to incubate overnight to make sure the cells were attached to the surface. After 24 hrs, 100 µL of HS-173 was added at the following final concentrations: $1.0x10^{-5}$ µM, $1.0x10^{-4}$ µM, $1.0x10^{-3}$ µM, $1.0x10^{-2}$ µM, 0.1 µM, 0.5 µM, 1 µM, 5 µM, 10 µM and 50 µM. Each concentration was added to a whole column in the plate (8 repetitions). As negative controls, 100 µL of growth medium without drug was added into wells containing cells, as well as DMSO control at the highest dose (0.05% v/v) to ensure inhibition was caused by HS-173 and not the diluent. Another column contained only medium and was used to calculate the background signal from the medium which was deducted from the results. After addition of inhibitors, the cells were incubated for 72 hrs. Then, 20 µL of 0.1 mg/mL Resazurin (Sigma-Aldrich Inc.) was added into each well, and the plate was incubated for 4 additional hrs. Absorbance was measured using a scanning multi-well spectrophotometer (VictorTM 3 1420 multi-label counter, Perkin Elmer, Waltham, MA, USA) at wavelengths of 560/590 nm. Background was controlled for by subtracting averaged blank values. The negative control was set to 100% viability, and the drug-treated samples were normalized to the negative control accordingly.

The measured, normalized values were analyzed using GraphPad Prism 8 (GraphPad software, Inc., La Jolla, CA, USA) by transforming the X-values logarithmically for further processing of the data. A normalized response – variable slope logistic nonlinear regression analysis was fitted to the data to calculate IC_{50} of HS-173 for each cell line. The resulting curves demonstrated the cell viability relative to the drug concentration. Three replicates were done for each cell line. IC_{50} values were used to establish four HS-173 concentrations to use for each cell line, shown in **Table 3.3**. These concentrations were designed to establish a therapeutic window of doses around each independent IC_{50} while still having two comparable doses across all cell lines.

Table 3.3- HS-173 concentrations for each cell line used for the duration of this thesis unless stated otherwise.

Cell Line	Concentrations used
H1	0.1 µM, 0.3 µM, 0.5 µM, 1.0 µM
H2	0.05 µM, 0.1 µM, 0.3 µM, 0.5 µM
H3	0.05 µM, 0.1 µM, 0.3 µM, 0.5 µM
H10	0.3 µM, 0.5 µM, 1.0 µM, 1.5 µM

3.4. Scratch Wound Healing Assay

The effect of HS-173 on the migratory capacity of the cell lines were studied using a live cell scratch wound assay. H1, H2, H3 and H10 cells were seeded in 8 replicates at a density of $3.0x10^4$ cells/well in Essen BioScience ImageLock 96-well plates (cat. no. 4379, Essen BioScience Ltd., Hertfordshire, UK) and allowed to incubate for 48 hrs to obtain confluent cultures. A wound-maker tool was used to create wounds within all wells, which were then washed 2 times with pre-warmed media. HS-173 was added in concentrations shown in **Table 3.3**, in addition to a control with only growth medium. Images were taken every 2 hrs for 72 hrs using the 10x objective in the IncuCyte Live Cell Imaging System (Essen BioScience Ltd.) with subsequent analyses performed using the IncuCyte Scratch Wound Cell Migration Software Module (cat. no. 9600-0012, Essen BioScience Ltd.) to find relative wound confluency. Each experiment was repeated three times.

3.5. Cell Morphology Imaging

H1, H2, H3 and H10 cells were seeded at $1.5x10^5$ cells/well and incubated for 24 hrs. HS-173 was then added to each cell line according to **Table 3.3** in addition to untreated cells. The cells were incubated for an additional 72 hrs. A Nikon TE2000 inverted light microscope (Nikon Instruments Inc., NY, USA) was used to capture images from each drug concentration using the 10X objective. Three representative images were taken from each well, and the experiments were repeated three times.

3.6. Western Blotting

Table 3.4- Reagents used for cell lysis.

Reagent Name	Company
RIPA Lysis Buffer	
Radioimmunoassay precipitation buffer (RIPA)	Thermo Fisher Scientific
10% Protease + Phosphatase inhibitors	
Protease + Phosphatase Inhibitors	
1 tablet protease inhibitors	Roche, Sigma-Aldrich Inc.
1 tablet phosphatase inhibitors	Roche, Sigma-Aldrich Inc.
1 mL RIPA Buffer	Thermo Fischer Scientific

Table 3.5- HS-173 concentrations for each cell line used for the western blot preparations.

Cell Line	Concentration of HS-173
H1	1.0 µM
H2	0.5 µM
H3	0.5 µM
H10	1.0 µM

To observe the inhibition effect of HS-173 on the PI3K pathway, cells from H1, H2, H3 and H10 cells treated with HS-173 were subjected to western blotting. Cells were seeded at $1.5x10^6$ cells/10 cm dish and treated after 24 hrs with concentrations of HS-173 shown in **Table 3.5**. Negative controls were grown in medium only. Cells were then washed twice with cold PBS, removed from the plates with a cell scraper and lysed after either 24, 48 or 72 hrs using RIPA buffer supplemented with 10% protease and phosphatase inhibitors. Cell debris was pelleted by spinning the samples at 13 500 x *g* for 10 mins at 4 °C. The protein concentration in each lysate was determined using a Pierce BCA Protein Assay Kit (Pierce Biotechnology, Rockford, lL, USA), then the samples were aliquoted and stored at −80 °C until use.

Table 3.6- Reagents used for running, transfer and blotting of SDS-PAGE.

Reagent Name	Company
1X Tris-glycine Running Buffer	
10X TGS buffer	Bio-Rad laboratories AB, Oslo, Norway
dH_2O	-
1X Tris-Glycine transfer buffer	
10X TG buffer	Bio-Rad laboratories AB
20% methanol	
dH_2O	-
Ponceau stain	
0.1% Ponceau	
Acetic Acid	
5% blocking buffer	
5% Skim milk powder	Bio-Rad laboratories AB
TBS-Tween Buffer	-
TBS-Tween Buffer	
10X TBS	-
0.1% Tween 20	
dH_2O	-
10X TBS (Tris-Buffered Saline)	
0.2 M Tris-HCl (pH 7.5)	Bio-Rad laboratories AB
1.5 M NaCl	Bio-Rad laboratories AB
dH_2O	-

Table 3.7- Antibodies used for immunostaining of SDS-PAGE.

Antibodies	Dilution	Company
Anti-Akt	1:1000	Cell Signaling, Danvers, MA, USA
Anti-p-Akt (Ser473)	1:1000	Cell Signaling
Anti-mTOR	1:1000	Cell Signaling
Anti-p-mTOR(Ser2448)	1:1000	Cell Signaling
Anti-GAPDH	1:10 000	Invitrogen, OR, USA
Secondary anti-rabbit mouse	1:10 000	Invitrogen

The samples were thawed on ice and 30 µg total protein of each sample was electrophoresed on either 6% or 10% Tris-Glycine SDS-polyacrylamide gels. Gels were run at

80 V for 30 min for protein stacking, and then at 100 V for protein separation, in Tris-glycine running buffer. Proteins separated on gels were blotted onto 0.2 µM pore nitrocellulose membranes (Bio-Rad laboratories AB) at 100 V for one hr (10% gel) or two hrs (6% gel) on ice using the BioRad Mini Trans-Blot transfer system and Tris-Glycine transfer buffer. Membranes were stained with Ponceau stain for 2 mins to visualize total protein bands before cutting to separate proteins of interest for blotting and blocking in 5% blocking buffer for 1 hr at room temperature on a see-saw rocker (Stuart Equipment, Cole-Parmer, Staffordshire, UK). Primary immunostaining on membranes was performed overnight at 4°C on a rocker using primary antibodies diluted in blocking buffer and against: Akt, p-Akt (Ser473), p-mTOR (Ser2448), mTOR and GAPDH. Membranes were washed 2 x 5 mins and 2 x 10 mins in TBS-Tween Buffer before adding secondary anti-rabbit mouse diluted 1:10 000 in blocking buffer for 1 hr at room temperature using a rocker. Membranes were then washed 4 x 5 mins and 2 x 10 mins before visualizing using the LAS3000 and chemiluminescent detection kit, either SuperSignal West Femto (Pierce Biotechnology) or SuperSignal West Pico (Pierce Biotechnology).

3.7. Flow Cytometry

3.7.1 Flow Cytometry Theory

Flow cytometry is a technique that can quantify cell properties including cell size, cell number, cell cycle and protein expression. Cells are stained with fluorophores/tagged antibodies or fluorescent dyes to detect proteins or other structures of interest.

Flow cytometry consists of three main components: fluidics, optics and electronics (**Fig. 3.1**). Initially the cell sample is taken up into the fluidics system and transported to the flow cell in a single cell suspension to pass through a laser beam. Having a single cell suspension is important in order to ensure investigation of individual cells or "events". The optical system is comprised of multiple lasers, filters, mirrors and detector lenses[144]. There are two illuminating lasers that determine non-fluorescent properties of the cells. Forward scatter (FSC), diffracted parallel from the light, determines the size of each cell. Side scatter (SSC), diffracted from 90^{o}, determines the internal complexity, or granularity, of each cell[145]. The rest of the lasers function to excite any fluorophores associated with each cell. All of these emissions are detected by a multitude of fluorescence detectors, or photomultiplier tubes (PMTs), and sent to the computer. The electronic system then digitizes the detected emissions to process into quantifiable data that can then be analyzed[144,145].

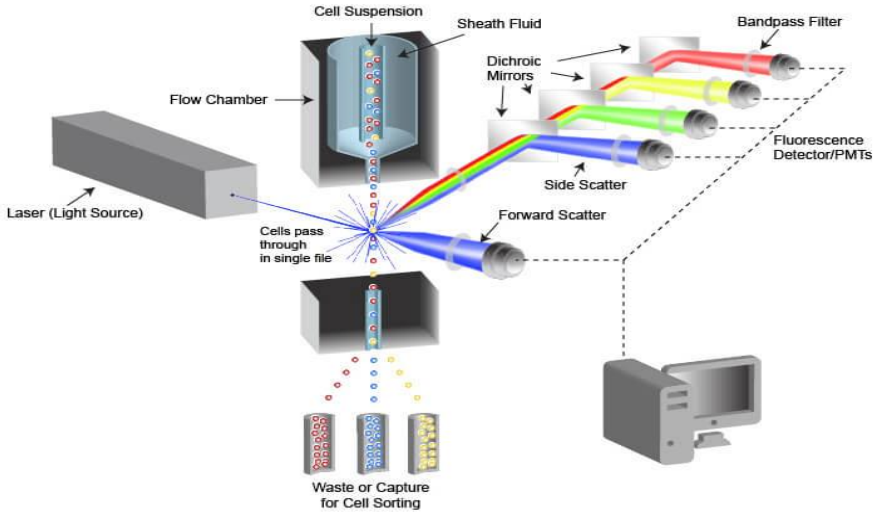

Figure 3.1: Schematics of a flow cytometer. Simplified diagram of the main components in a flow cytometer. Samples enter from the top as a cell suspension through the flow chamber and are arranged into single file as they pass through the laser (light source). Each cell scatters light as forward scatter (FSC) and side scatter (SCC), and emits fluorescent light if tagged with a fluorophore. Dichroic mirrors act to filter specific wavelengths to the proper detectors. Detected emissions are transferred to the processing system. Analyzed cells may be either sorted based on fluorescent characteristics or passed into a waste bin. Schematic from *https://www.cellsignal.com/contents/_/overview-of-flow-cytometry/flow-cytometry-overview*

In multiplexed experiments, where cells are tagged with more than one fluorophore, a mathematical method called compensation is required prior to analysis.

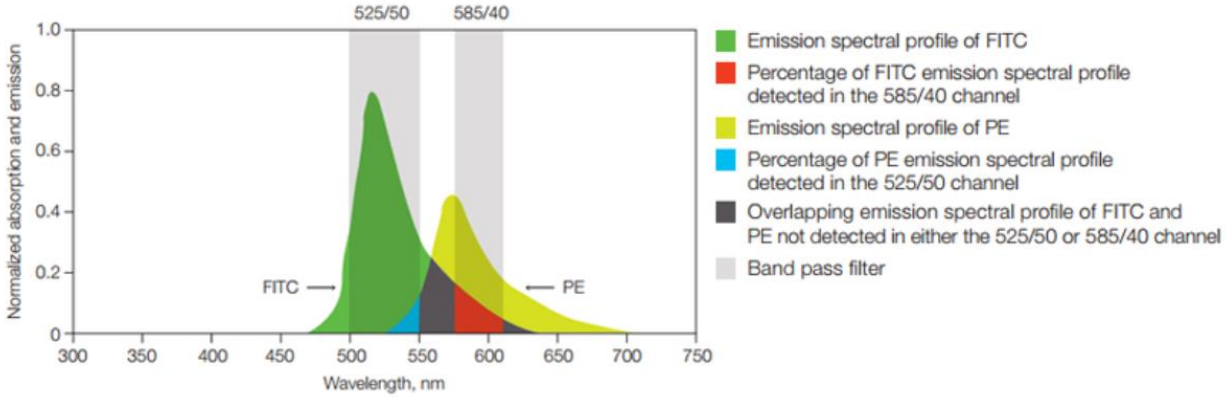

Figure 3.2: Emission spectra and compensation of FITC and PE. The emission spectra of FITC and PE, and representation of their spillover captures by each respective filter. Blue shows the spillover from PE into FITC detection, and red represents spillover from FITC into PE detection. Single FITC and PE stained samples would be analyzed to determine these values and subtract from each sample. *https://www.bio-rad-antibodies.com/flow-cytometry-fluorescence-compensation.html*

Fluorophores often have some overlap in their emission spectra that can be registered in a detector meant for another fluorochrome, a phenomenon known as spillover (**Fig. 3.2**). This

overlap, if not controlled for, can skew data and give false readings in different fluorescence channels. Therefore, when using more than one fluorophore, controls are required for proper analysis. To properly determine the amount of overlap in fluorophores used, a compensation matrix is made to control for any spillover in the final analysis. Single fluorophore controls are used (i.e. FITC only, PE only) and the software can then calculate the overlap and normalize the data accordingly[146].

3.7.2 Apoptosis Assay

An apoptosis assay was performed to assess the apoptosis-inducing ability of HS-173 on the H1, H2, H3 and H10 cell lines. To detect the stages of apoptosis of the cells, FITC-tagged Annexin V and propidium iodide (PI) were analyzed. Annexin V, a phospholipid-binding protein, has a high binding affinity to phosphatidyl serine (PS) which is located on the internal leaflet of the membrane in viable cells. PI is a membrane-impermeable nucleic acid binding dye.

In viable cells, neither stain will bind as PS and nucleic acids are located inside the cell. In early apoptosis, the membrane is still intact, but PS has shifted to the external membrane, therefore the cells will be FITC +. In late apoptosis, the membrane is breaking down, and is therefore permeable by PI, therefore these cells will be FITC +/ PI +. If cells are necrotic, there is a complete membrane breakdown and cells may only be PI +. However, it is difficult to distinguish between late apoptotic and necrotic cells; therefore these categories was combined for analysis[147].

Cells were seeded at a density of $1.2x10^5$ cells/well in six-well plates (Nunc). After 24 hrs, cells were treated with doses as shown in **Table 3.3** for 72 hrs. Culture medium was removed and collected and rinsed two times with cold PBS. As a positive control for apoptosis, 4 µL of 30% H_2O_2 was added to one well per cell line for 2 hrs. Cells were trypsinated, collected and centrifuged at 900 rpm for 4 mins. Following this cell pellets were then rinsed with cold PBS and centrifuged a second time at 900 rpm for 4 mins. 200 µL of 1X Annexin V binding buffer was added into each sample, followed by staining using 5 µL of AlexaFluor488 Annexin and 1uL of propidium iodide (PI; AlexaFluor®488 Annexin v/dead cell apoptosis kit; Molecular Probes, Life Technologies). Untreated cell controls included: PI staining only, Annexin-FITC staining only, no staining, and double staining apoptosis positive control. Samples were placed on ice before being analyzed using a BD LSR Fortessa flow cytometer (BD Bioscience). Data analysis was performed using FlowJo 10.6.1 (Tree Star Inc., Ashland, OR, USA). Cells were gated as shown below.

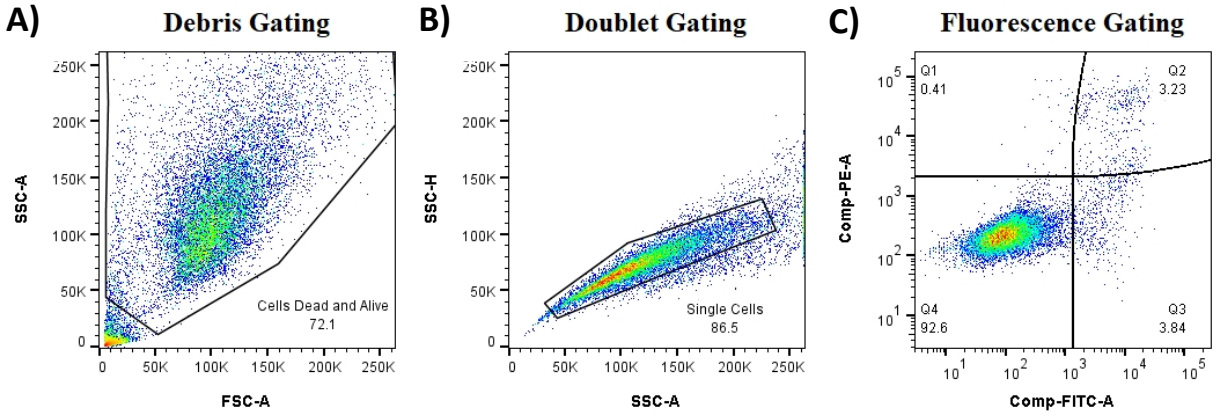

Figure 3.3: Gating path for flow samples. A) Gating out debris. This gate is set to include all live cells as well as possible dead cells and apoptotic bodies. B) Gates out doublets. This gate is also set wide to accommodate for increase granularity and size distribution of apoptosing cells. C) Gating of fluorescence quadrants based on single stain controls and confirmed populations with positive dead cell control.

3.9. Statistical Analysis

All statistical analyses were done using GraphPad Prism v8 (GraphPad Software, Inc.). Scratch wound data were analyzed using an ordinary one-way ANOVA with Dunnett's multiple comparisons test, and flow data were analyzed with an ordinary two-way ANOVA with Dunnett's multiple comparisons test. A p value ≤ 0.05 was regarded as statistically significant.

4.0 Results

4.1 Viability Assays

4.1.1 HS-173 effectively decreases cell viability

A resazurin cell viability assay was performed to determine the IC_{50} doses of HS-173 in our four cell lines by exposing them to increasing drug concentrations during a 72 hrs incubation period.

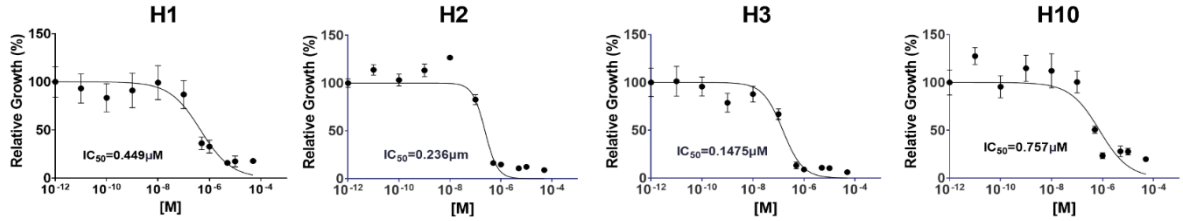

Figure 4.1: Representative dose-response curves of H1, H2, H3 and H10 cell lines after exposure to increasing doses of HS-173 for 72 hr. Cells were seeded in a 96 well format at $5x10^3$ cells/well. After 24 hr, HS-173 was added in increasing concentrations from 0.01nM – 50µM. After 72 additional hr, viability was assessed using a resazurin assay. The experiments were performed in triplicate, n=6 in each experiment.

As shown in **Fig. 4.1,** HS-173 reduced the cell viability in all four cell lines in a dose-dependent manner, even at nM concentrations. All cell lines displayed a consistent response to the inhibitor, although H2 and H3 viability declined rapidly once concentrations surpassed 0.1 µM and viability remained extremely low at all higher concentrations. Regarding the H1 and H10 cells, the sigmoidal curve fit was not as steep as for H2 and H3 cells, indicating higher resistance towards drug treatment. This was also reflected in the IC_{50} doses (**Table 4.1**).

Table 4.1: Mean IC_{50} doses of each cell line following the 72 hrs resazurin viability assay. N=3.

Cell Line	Mean IC_{50}±SD [µM]
H1	0.60±0.41
H2	0.23±0.05
H3	0.15±0.005
H10	1.00±0.45

Table 4.1 displays the calculated mean IC_{50} doses of all cell lines. IC_{50} is defined as the concentrations where 50% of cell growth is inhibited. These results were consistent across cell lines, ranging from 0.15-1.0 µM. H2 was the most sensitive to the drug, while H10 was the most resistant. All cell lines were susceptible to the drug at very low concentrations. These

IC_{50} doses were utilized to establish a range of effective doses tailored to each cell line in subsequent assays, while keeping two doses comparable across all cell lines.

4.1.1 HS-173 induces morphology changes across all cell lines

The effects of HS-173 on cell morphology of H1, H2, H3 and H10 cell lines were studied by light microscopy.

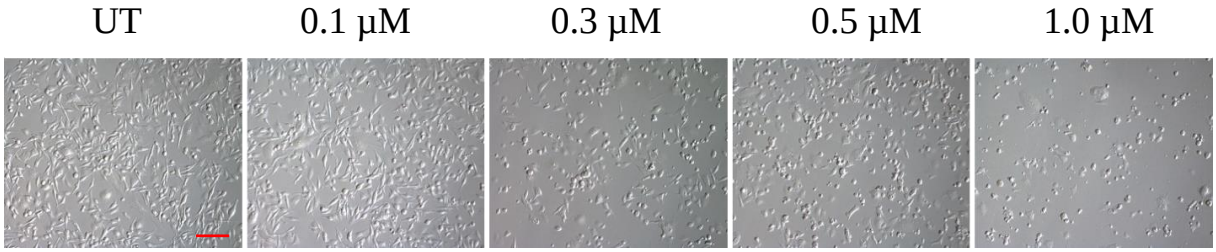

Figure 4.2: Images demonstrating H1 cell morphology changes under presence of increasing concentrations of HS-173. Cells were seeded in 6-well plates and exposed to HS-173. Images were taken with a Nikon TE2000 inverted microscope after 72 hrs of treatment. Scale bar=300 µm. UT: Untreated

In general, the cell density decreased with increasing doses of HS-173. Untreated H1 cells (**Fig. 4.2)** exhibited an adherent, elongated and spindle-like morphology with smooth membranes. At 0.1 µM, changes in cell morphology were not seen, however at 0.3 µM, cells begin to lose their adherence, and those still adhered have fewer appendages. At 0.5 µM, large amounts of floating cells were apparent, and adhered cells exhibited more rounded cell-shapes, as well as more granular membranes. At the highest concentration, 1.0 µM, cell debris could be seen floating in the media, in addition to non-adherent cells. The few cells that still adhered were flat with granular membranes, and almost no spindle-like appendages were visible.

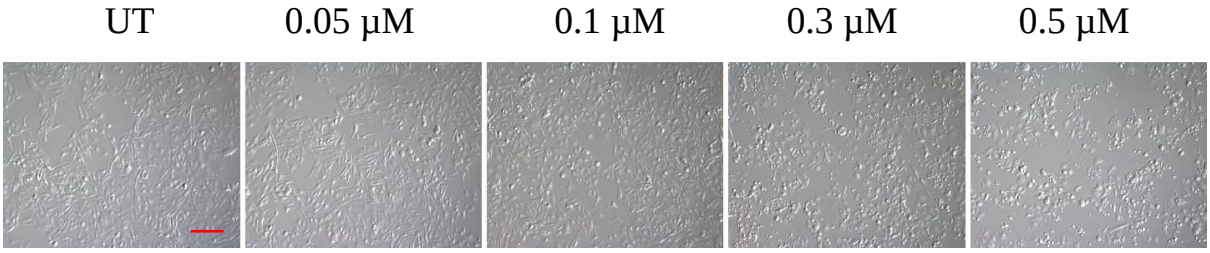

Figure 4.3: Images demonstrating H2 cell morphology changes under presence of increasing concentrations of HS-173. Cells were seeded in 6-well plates and exposed to HS-173. Images were taken with a Nikon TE2000 inverted microscope after 72 hrs of treatment. Scale bar=300 µm. UT: Untreated.

Untreated H2 cells **(Fig 4.3)** showed a similar morphology to untreated H1 cells, although they were a bit flatter and had much more visible cellular structures. At the lowest concentrations, 0.05 µM, there were no visible morphological changes. At 0.1 µM, although there were a few cells that started to lose their spindle-like morphology, the majority of cells

looked similar to the control. Cells treated with 0.3 µM exhibited a large population of floating cells, as well as debris floating in the growth medium. Cells that were adhesive had both spindle-like and rounded morphology. At the highest concentration, 0.5 µM, the cell morphology was similar to 0.3 µM, lots of floating cells and cell debris, as well as a population of adhered cells, although at this concentration there was a noticeably smaller number of cells.

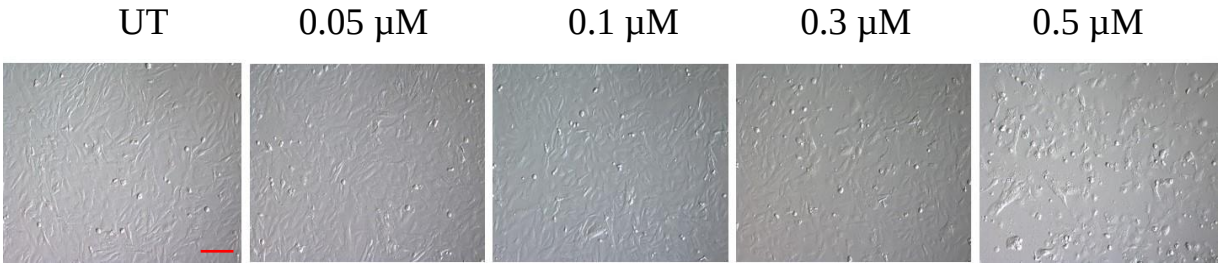

Figure 4.4: Images demonstrating H3 cell morphology changes under presence of increasing concentrations of HS-173. Cells were seeded in 6-well plates and exposed to HS-173. Images were taken with Nikon TE2000 inverted microscope after 72 hrs of treatment. Scale bar=300 µm. UT: Untreated.

Untreated H3 cells **(Fig 4.4)** were flat fibroblast-like cells, with a granular membrane, and although they did not show as extensively spindle-like structures as seen for H1 and H2 cells, they were quite elongated. They also formed a tight monolayer of cells with little space in between each cell. The lowest concentrations, 0.05 µM, showed no major morphological changes. Wells treated with 0.1 µM had some floating cells visible, and adherent cells started pulling away from each other to form a space in between single cells instead of a tight monolayer like seen for the untreated cells. Those treated 0.3 µM however, showed a more extreme case of this, with a higher amount of floating cells, and a more scattered adherent cell growth. At the highest concentration, 0.5 µM, there were much less cell adhered than in the control, and there was also a very large amount of small cell debris scattered along the bottom of the plate. Adhered cells also exhibited a rounding of the membrane, although there were still cells that displayed the typical elongated form.

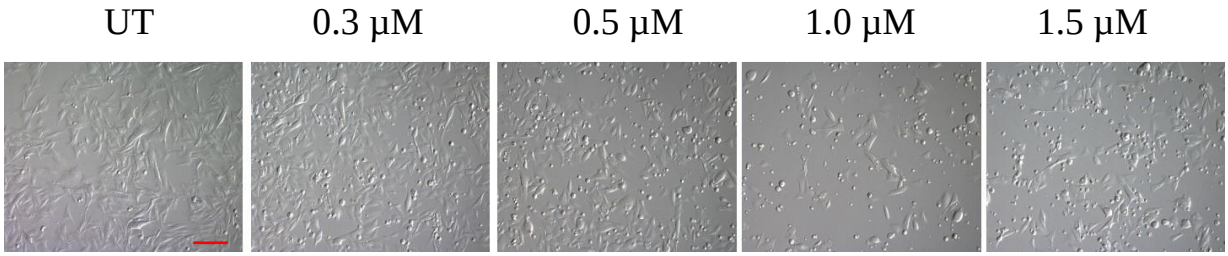

Figure 4.5: Images demonstrating H10 cell morphology changes under presence of increasing concentrations of HS-173 after 72 hrs. Cells were seeded in 6-well plates and exposed to HS-173. Images were taken with Nikon TE2000 inverted microscope after 72 hrs. Scale bar=300 µm. UT: Untreated.

Untreated H10 cells **(Fig 4.5)** also showed a fibroblast-like morphology, with spindle features and a relatively flat cell shape. They also grew in a sporadic, overlapping manner, unlike the H3 cells. Even at the lowest dose of HS-173, 0.3 µM, there was a much higher amount of rounded, floating cells, but the adhered cells still seemed relatively unaffected. At 0.5 µM much of the same was seen, a large amount of floating cells, and the adhered cells started to take on a slightly less elongated shape and had a shortened oblong morphology. The appearance at 1.0 µM was similar to 0.5 µM with a lower cell density. There was not a noticeable difference between the final two concentrations 1.0 µM and 1.5 µM. Interestingly, unlike the other cell lines, although there were many cells floating, the amount of floating and adhered cells combined was not noticeably different than the control, where in the other cell lines we saw a marked decrease in the cells overall. In H10, there seemed to be still many whole cells in the media, and less debris compared to the other three cell lines.

4.2 HS-173 decreases cell proliferation and migration in H1, H2, H3 and H10 cell lines

To assess the effect of HS-173 on the proliferation and migration of all cell lines, a wound-healing assay was performed.

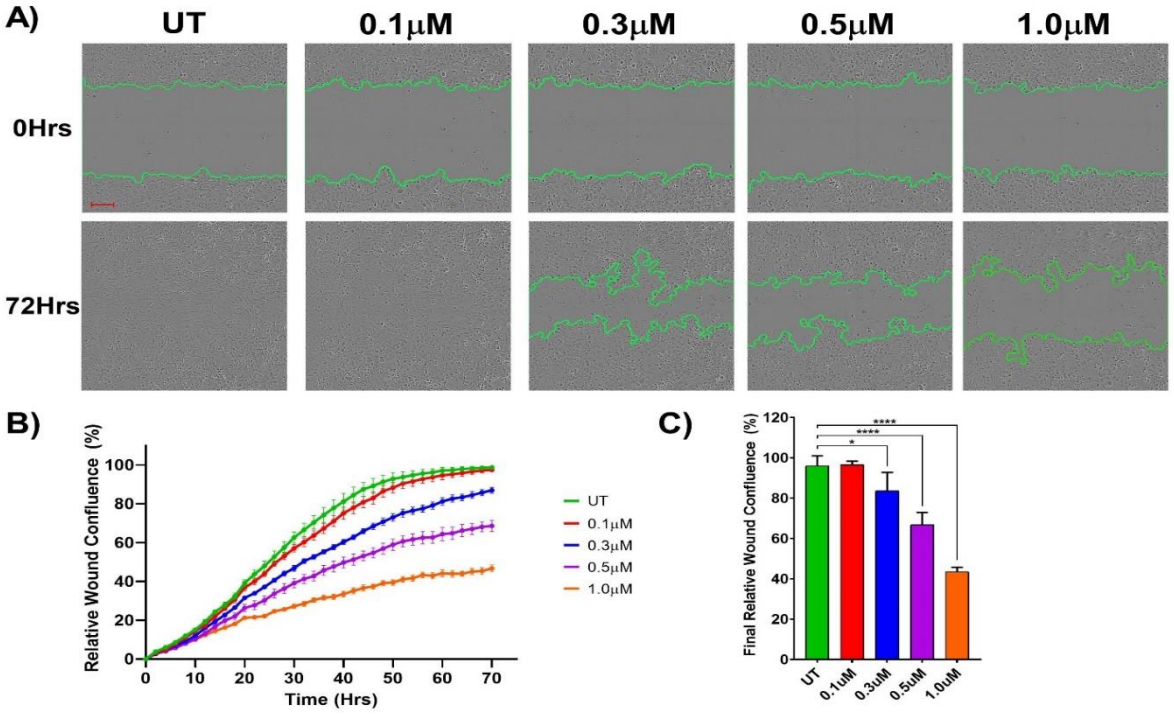

Figure 4.6: Migration of H1 cells during exposure with varying concentrations of HS-173. Cells were seeded at 30 000 cells/well in 96-well dishes and increasing concentrations of HS-173 were added just prior to time lapse imaging. A) Representative images from 0 hrs and 72 hrs of each drug concentration. Images were taken every 2 hrs for 72 hrs. Green line represents wound edge, generated by Incucyte software. B) Quantification of wound confluence over 72 hrs for each treatment group. C) Final relative wound confluence of all treatment groups. Experiments were carried out in triplicate,

As seen in **Fig. 4.6. A**, untreated H1 cells fully closed the wound created after around 50 hrs and reached a plateau of growth over the rest of the experiment. Cells outside the scratch were quite confluent and floating cells were observed, similar to what is typical in a confluent cell culture flask. The cells that migrated over the wound were elongated with a smaller amount of floating or rounded cells. At the lowest dose, 0.1 µM, the wound was closed entirely although it did take slightly longer than in the untreated **(Fig. 4.6 B)**. Visually, there were much more rounded cells in the sample. Wells treated with the highest three concentrations did not successfully close the gap, and as the drug concentration increased, the migration into the wound lowered significantly (**Fig. 4.6 C**). There was also a very noticeable difference in cell morphology; the cells were almost all rounded. At the highest dose, 1.0 µM, the outer cells had an even lower confluency than at the initial timepoint.

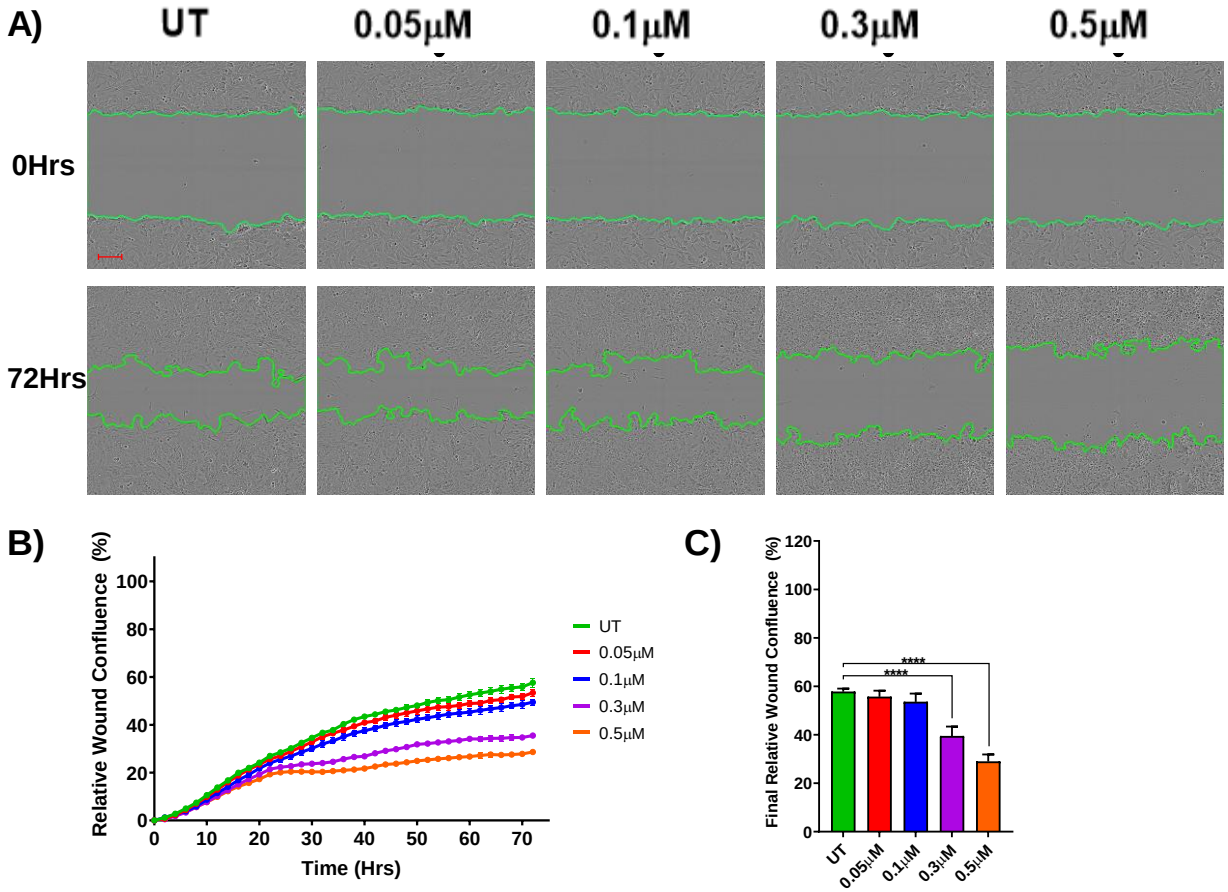

Figure 4.7: Migration of H2 cells during exposure with varying concentrations of HS-173. Cells were seeded at 30 000 cells/well in 96-well dishes and increasing concentrations of HS-173 were added just prior to time lapse imaging. A) Representative images from 0 hrs and 72 hrs of each drug concentration. Images were taken every 2 hrs for 72 hrs. Green line represents wound edge, generated by Incucyte software. B) Quantification of wound confluence over 72 hrs for each treatment group. C) Final relative wound confluence of all treatment groups. Experiments were carried out in triplicate, n=6 per concentration. Abbreviations: UT: Untreated. ****: $p<0.0001$. Scale bar=150 µm.

Untreated H2 cells were unable to close the wound over the course of 72 hrs. Visually, the cells seemed to instead layer on top of each other on the outer edges instead of migrating inwards, to the point that making out individual cells was difficult (**Fig. 4.7 A**). Because of this extremely confluent monolayer, there was quite a noticeable amount of cell debris and round cells on the outer edges, although more towards the center of the well, single elongated H2 cell were apparent. Cells exposed to 0.05 µM had barely any qualitative differences compared to the untreated cells, and although 0.1 µM samples had a non-significant variability in wound closure (**Fig. 4.7 B, C**), the outer cells were much more granular and rounded. Exposure to the two highest doses resulted in both a significant difference in wound closure and morphology. Cells in the monolayer had barely any "typical" H2 morphology visible, as all cells were extremely rounded and granular.

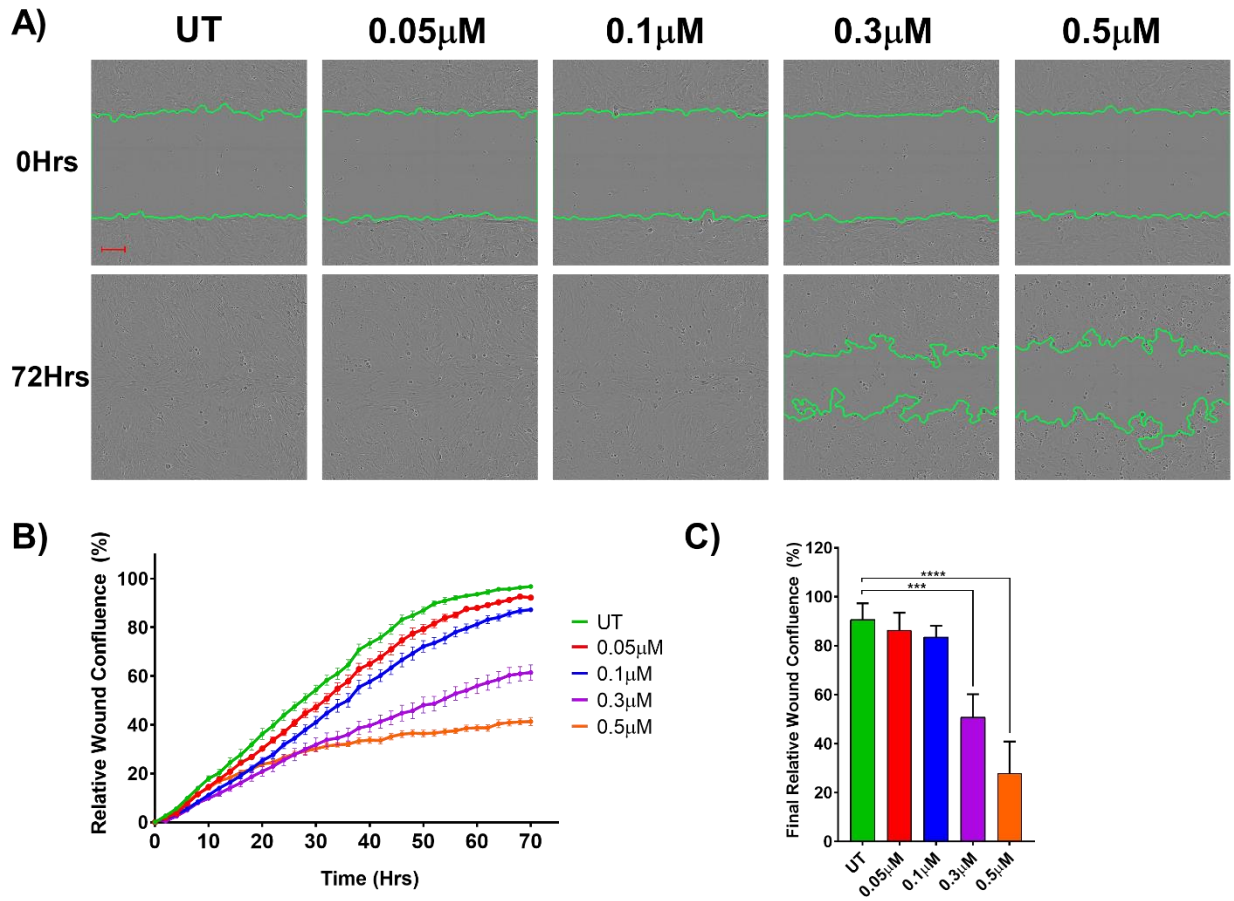

Figure 4.8: Migration of H3 cells during exposure with varying concentrations of HS-173. Cells were seeded at 30 000 cells/well in 96-well dishes and increasing concentrations of HS-173 were added just prior to time lapse imaging. A) Representative images from 0 hrs and 72 hrs of each drug concentration. Images were taken every 2 hrs for 72 hrs. Green line represents wound edge, generated by Incucyte software. B) Quantification of wound confluence over 72 hrs for each treatment group. C) Final relative wound confluence of all treatment groups. Experiments were carried out in triplicate, n=6 per concentration. Abbreviations: UT: Untreated. ****: $p<0.0001$, ***: $p<0.001$. Scale bar=150 µm

Untreated H3 cells fully closed the wound and phenotypically, untreated, 0.05 µM-treated, and 0.1 µM-treated cells were very similar. H3 cells had a consistent confluency and morphology for both those that filled the wound and those on the outer frame (**Fig. 4.8 A**), although when quantified, 0.05 µM and 0.1 µM resulted in slightly slower wound closures (**Fig. 4.8 B**). Cells treated with 0.3 µM had a significant drop in wound closure compared to the control as well as those treated with 0.5 µM (**Fig. 4.8 C**). H3 cells treated at 0.5 µM displayed a very different morphology to what was seen in untreated cells, which also reflects what was seen in **Fig. 4.4.**

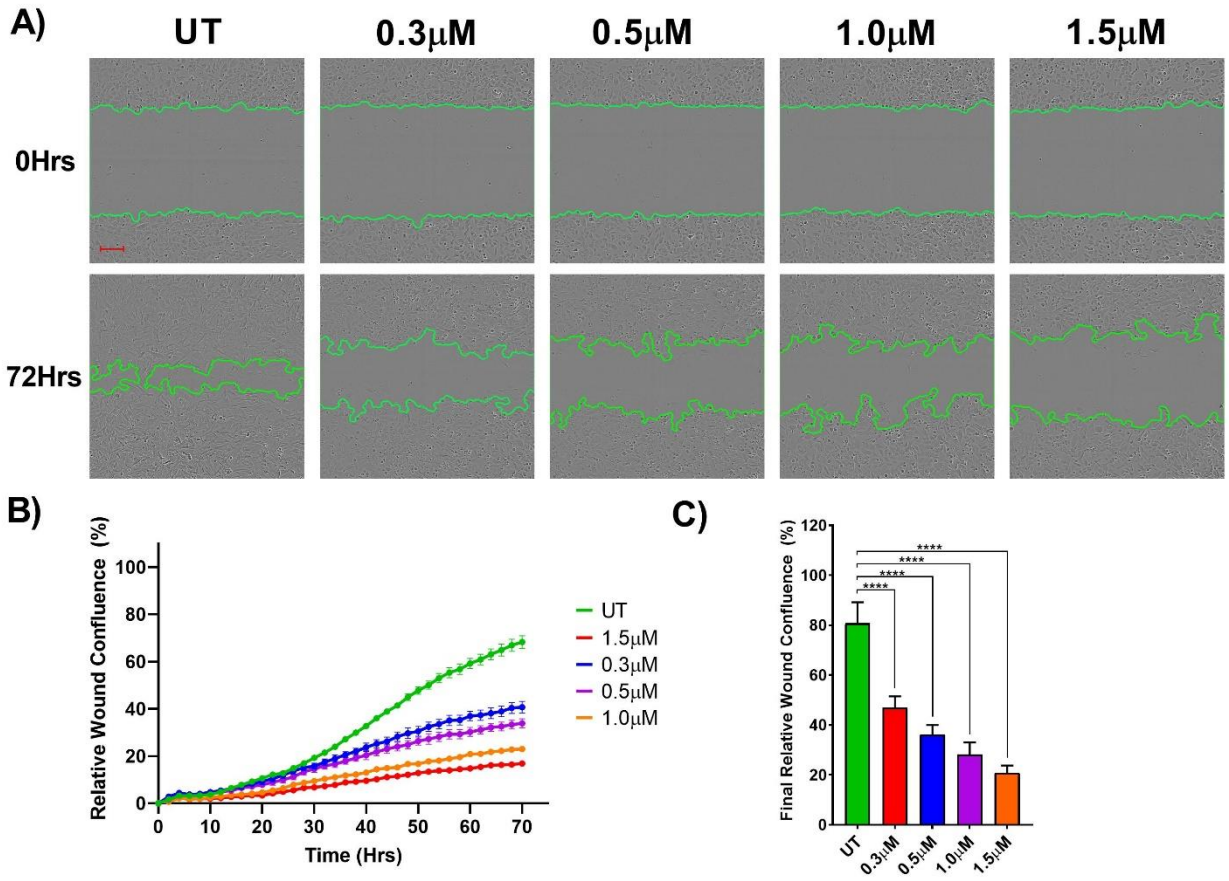

Figure 4.9: Migration of H10 cells during exposure with varying concentrations of HS-173. Cells were seeded at 30 000 cells/well in 96-well dishes and increasing concentrations of HS-173 were added just prior to time lapse imaging. A) Representative images from 0 hrs and 72 hrs of each drug concentration. Images were taken every 2 hrs for 72 hrs. Green line represents wound edge, generated by Incucyte software. B) Quantification of wound confluence over 72 hrs for each treatment group. C) Final relative wound confluence of all treatment groups. Experiments were carried out in triplicate, n=6 per concentration. UT: Untreated. Abbreviations: ****: $p<0.0001$. Scale bar=150 µm

Untreated H10 cells did not close the wound entirely after 72 hrs. The outer cell growth was extremely confluent (**Fig. 4.6 A)**, however the migration of the cells into the wound only reached 80% of maximum. The cells after 72 hrs still had a very typical elongated fibroblast-like shape. Even the cells treated with the lowest dose, 0.3 µM, the wound closure was visibly slower than the untreated control. It was difficult to see the base layer of cells, however similar to **Fig. 4.5** there were many round cells compared to the untreated cells, although it was difficult to tell if these were floating. As the dosages increased, there was less of a tightly formed monolayer surrounding the wound and it was possible to see the more oblong shape of adhered cells. In **Fig. 4.6 B**, the untreated cells had a slow but semi-logarithmic growth curve, whereas all treated samples had a flat line with a very low slope. The final wound confluence (**Fig. 4.6 C)** showed extremely significant reduction of wound closure at all concentrations.

4.3 HS-173 induces apoptosis in H1, H2, H3 and H10 cell lines

An apoptosis assay was performed to determine if HS-173 causes the melanoma metastases cell lines to undergo apoptosis, and possibly explain the morphological changes the cells underwent after exposure.

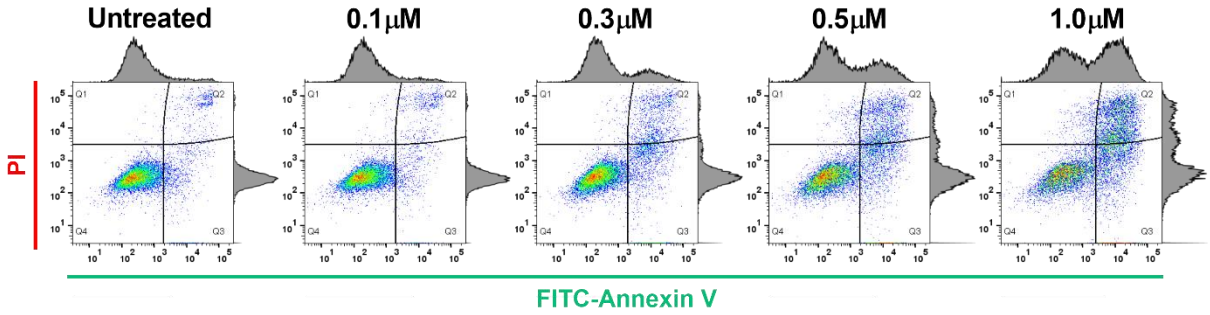

Figure 4.10: Flow cytometric analysis of apoptotic profile after treatment of H1 with increasing concentrations of HS-173. Dot plots are representative samples of H1 fluorescent profile after treatment for 72 hrs of 0.1 μM, 0.3 μM, 0.5 μM and 1.0 μM of HS-173. FITC-Annexin V labels cells undergoing early apoptosis, and PI labels late apoptotic/necrotic cells. Experiments were performed in triplicate. Abbreviations: Q1: necrotic cells, Q2: late apoptotic cells, Q3: early apoptotic cells, Q4: viable cells.

The apoptosis profile of untreated H1 cells **(Fig. 4.10)** was a typical healthy cell culture with total apoptosis and necrosis below 10%. As HS-173 concentrations increased, the surviving cells decreased and there were much larger populations in the apoptotic quadrants, although there was not a large population of necrotic cells as the inhibitor concentration increased. The lowest concentration (0.1 μM) had no visual differences in apoptotic profile but starting at 0.3 μM the apoptosis in the population was clearly higher than untreated control.

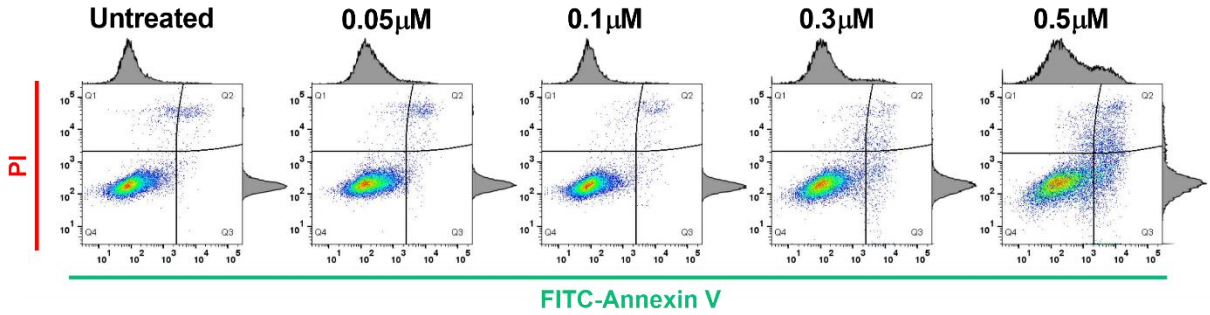

Figure 4.11: Flow cytometric analysis of apoptotic profile after treatment of H2 with increasing concentrations of HS-173. Dot plots are representative samples of H2 fluorescent profile after treatment for 72 hrs of 0.05 μM, 0.1 μM, 0.3 μM, and 0.5 μM of HS-173. FITC-Annexin V labels cells undergoing early apoptosis, and PI labels late apoptotic/necrotic cells. Experiments were performed in triplicate. Abbreviations: Q1: necrotic cells, Q2: late apoptotic cells, Q3: early apoptotic cells, Q4: viable cells.

H2 untreated cells **(Fig. 4.11)** also showed less than 10% of total apoptotic and necrotic cells. For the first two drug concentrations (0.05 μM, 0.1 μM) the apoptotic profile was not

entirely discernible from the untreated control, however at 0.3 µM there was a shift of the cell population into early and late apoptosis. Although 0.5 µM had much more apoptotic cells than the untreated control, there were no clear dense population in either Q2 or Q3.

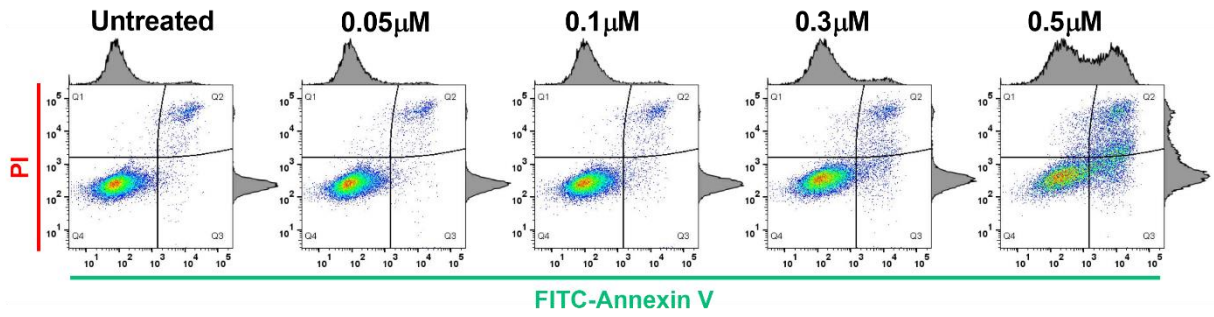

Figure 4.12: Flow cytometric analysis of apoptotic profile after treatment of H3 with increasing concentrations of HS-173. Dot plots are representative samples of H3 fluorescent profile after treatment for 72 hrs of 0.05 µM, 0.1 µM, 0.3 µM, and 0.5 µM of HS-173. FITC-Annexin V labels cells undergoing early apoptosis, and PI labels late apoptotic/necrotic cells. Experiments were performed in triplicate. Abbreviations: Q1: necrotic cells, Q2: late apoptotic cells, Q3: early apoptotic cells, Q4: viable cells.

The H3 cells **(Fig. 4.12)** had a similar profile to the H2 cells. Treatments with 0.05 µM or 0.1 µM did not result in noticeably larger populations of apoptotic cells than those in the untreated control, but at 0.3 µM there was a shift of the population into both early and late apoptosis. The highest concentration at 0.5 µM however did show clear populations of both early and late apoptotic cells, while the majority of the population was still viable according to the density of the dot plot.

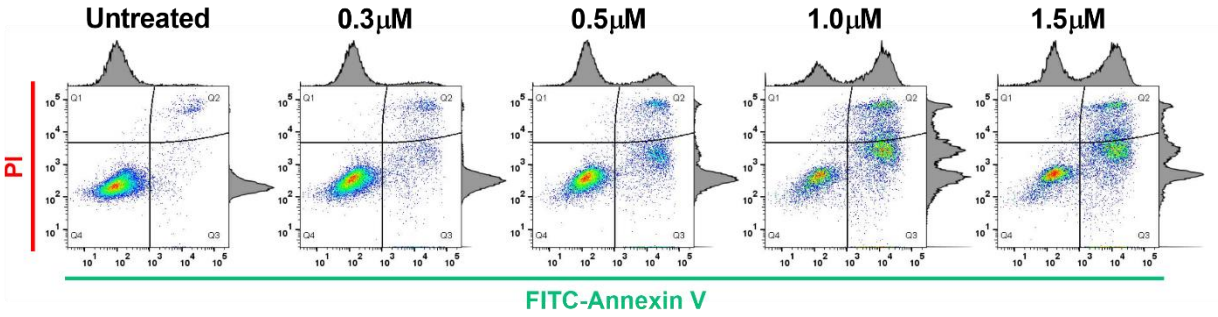

Figure 4.13: Flow cytometric analysis of apoptotic profile after treatment of H10 with increasing concentrations of HS-173. Dot plots are representative samples of H10 fluorescent profile after treatment for 72 hrs of 0.3 µM, 0.5 µM, 1.0 µM and 1.5 µM of HS-173. FITC-Annexin V labels cells undergoing early apoptosis, and PI labels late apoptotic/necrotic cells. Experiments were performed in triplicate. Abbreviations: Q1: necrotic cells, Q2: late apoptotic cells, Q3: early apoptotic cells, Q4: viable cells.

All H10 samples **(Fig. 4.13)** with HS-173 pre-treatment had a visible difference in apoptotic profile compared to the control. While the lowest concentration, 0.3 µM, only showed

marginal differences, there were distinct cell populations in both early and late apoptotic phases. While these populations did increase in number as the concentration increased, there was not a very large change between 1.0 µM and 1.5 µM despite the large change in concentration. Interestingly, despite the large amounts of apoptotic cells, there was not a marked increase in necrotic cells.

The decrease in cell viability, or increase in apoptosis, reflected the results seen in the scratch wound. The drug had a significant effect on cell function at the two highest doses across all cell lines (**Fig. 4.14**). In H1 and H3, cell viability was decreased to around 60% at the highest dose, whereas in H2, 70% of cells survived the highest treatment of HS-173. H10 was extremely susceptible in all doses except 0.3 µM. Cells treated at 1.0 µM and 1.5 µM both had around 40% of viable cells. Overall, the apoptosis was less than expected in H1 and H2 based on the IC_{50} results, but it should be noted that IC_{50} does not necessarily reflect the concentration at which 50% of cells are dead.

4.4 HS-173 effects reduce activation of major proteins in PI3K pathway

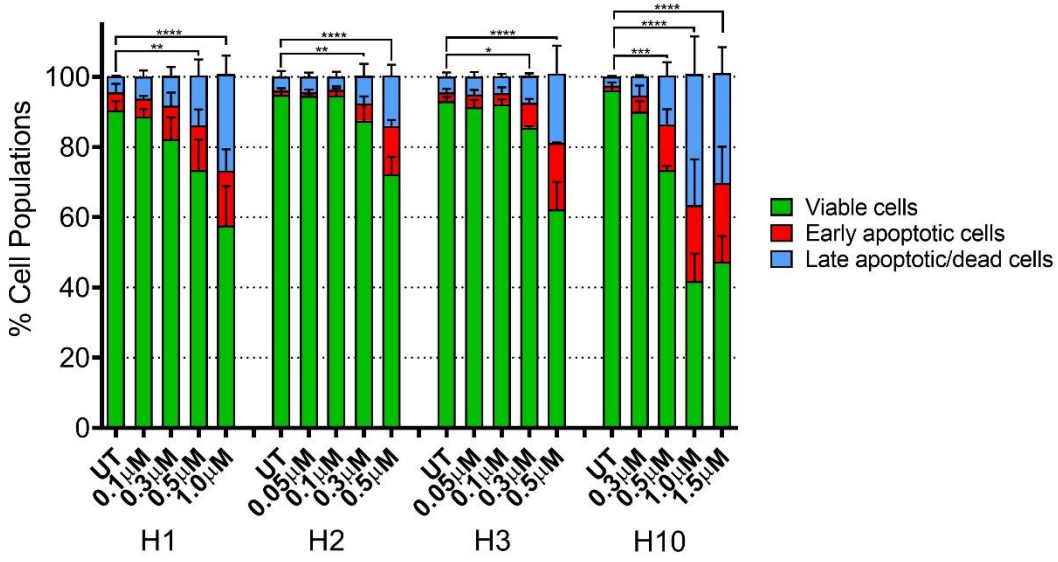

Figure 4.14: Quantification of apoptotic profile after treatment of all cell lines with increasing concentrations of HS-173. Percentage of viable, early apoptotic and late apoptotic/dead cells was calculated for H1, H2, H3 and H10 cell lines. Two-way ANOVA compared viable populations between each drug concentration and untreated control. Abbreviations: * $p < 0.05$, ** $p < 0.01$, ***, $p < 0.001$****: $p < 0.0001$.

Western blotting was performed to assess the actual effect of HS-173 on key proteins in the PI3K pathway. Three different timepoints were used to visualize the inhibitory effects of the drug. Unfortunately, due to coronavirus restrictions, there was only time to perform the 72

hrs timepoint for H3, and there was only time to perform one experiment per cell line. It is also important to note that H3 only had 20 µg of protein added, while optimized H1, H2 and H10 had 30 µg.

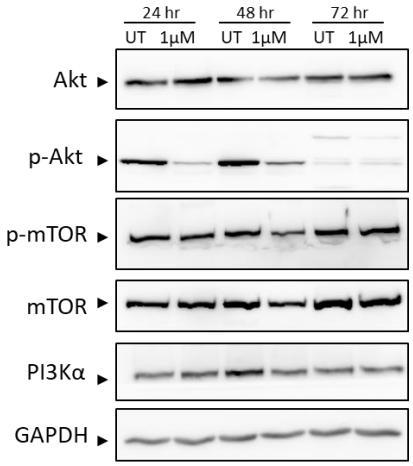

Figure 4.15: Expression of PI3K pathway proteins in H1 cells after treatment with 1.0 µM HS-173 for 24 hrs, 48 hrs and 72 hrs. N=1.

According to **Fig. 4.15**, the effect of HS-173 on H1 cells was mainly seen in the phosphorylation of Akt, across all three time points. Akt remained unchanged in both treated and control, however there was a very large decrease in the phosphorylated protein even as early as 24 hrs. After 72 hrs, there were several non-specific bands detected. HS-173 did not appear to have a large effect on phosphorylation of mTOR, although there was a slight decrease

in detection after 48 hrs in the treated sample. PI3K also had relatively consistent expression PI3Kα, but similarly to mTOR, expression was slightly lower in the 48 hrs time point.

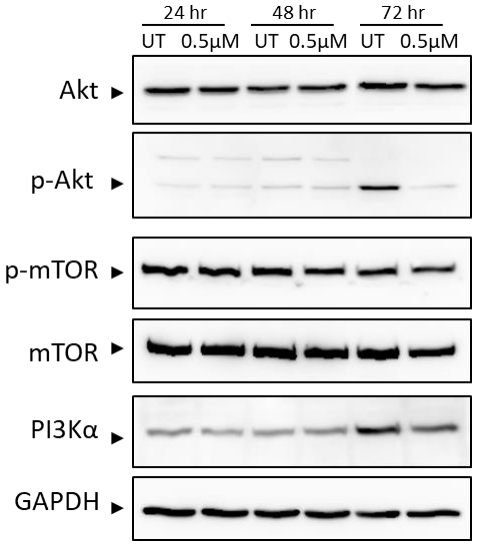

Figure 4.16: Expression of PI3K pathway proteins in H2 cells after treatment with either 0.5 μM of HS-173 for 24 hrs, 48 hrs and 72 hrs. N=1.

As shown in **Fig. 4.16,** the major effect of HS-173 on H2 cells could be detected in the phosphorylation of Akt. The effect seemed the most prevalent at the 72 hrs timepoint, where there was a clear decrease in the amount of p-Akt in the treated cells compared to untreated cells, while the unphosphorylated Akt did not change. Again similar to H1, there was some non-specific banding in the earlier timepoints in both control and treated samples. Both unphosphorylated and phosphorylated mTOR expression was consistent across treatments and samples. PI3Kα also showed some reduced expression in the 72 hrs timepoint, consistent with the p-Akt results.

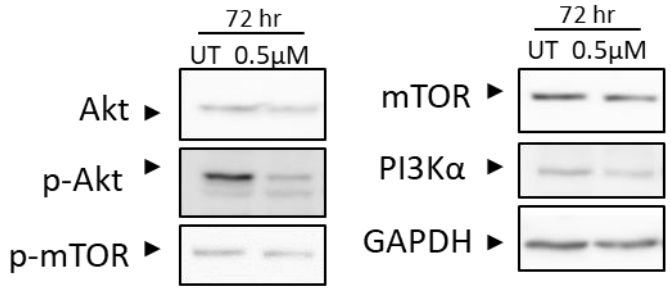

Figure 4.17: Expression of PI3K pathway proteins in H3 cells after treatment with either 0.5 μM of HS-173 for 72 hrs. N=1.

Unfortunately due to coronavirus-related time constraints, **Fig. 4.17** only showed the 72 hrs time point of H3 proteins instead of the dynamics over three days. However, it was still clear that Akt phosphorylation was reduced even after 72 hrs. There is also possibly a very small decrease in p-mTOR and PI3K although it is extremely small and difficult to confirm.

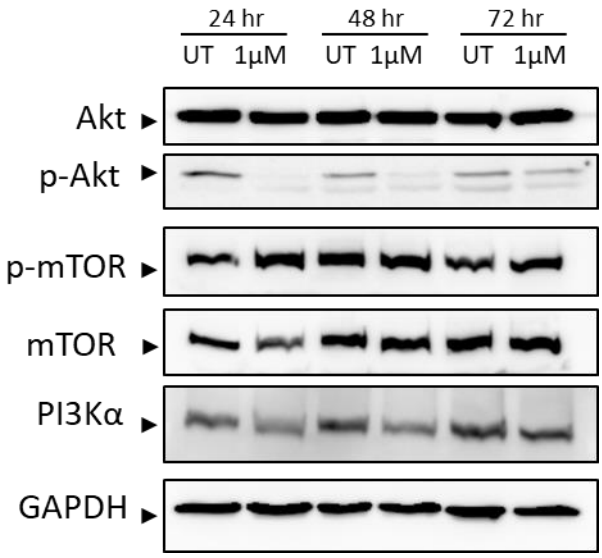

Figure 4.18: Expression of PI3K pathway proteins in H10 cells after treatment with either 1.0 μM of HS-173 for 24 hrs, 48 hrs and 72 hrs. N=1.

H10 cells had an immediate reduction in Akt phosphorylation after 24 hrs, although the expression slowly recovered over the next two time points (**Fig. 4.18**). There were no major changes in the other protein level expressions, although it seemed that phosphorylation of mTOR was slightly increased at 24 hrs and leveled off as time continued, and PI3Kα had a slight decrease in 24 hrs and 48 hrs, but again recovered after 72 hrs.

5.0 Discussion

Brain metastases are an extremely fatal and common outcome for patients with advanced melanoma. Around 70% of melanoma patients develop brain metastasis[79], and the survival is measured in a few months after diagnosis, even with the most extensive treatment[80]. Current treatments are not effective, among others due to poor drug penetration through the blood-brain barrier, these tumours are inherently radioresistant and they develop treatment resistance after a few months[103]. Thus, advancements in treatments such as targeted therapeutics are urgently required.

In this thesis, we show that the selective PI3Kα inhibitor HS-173 effectively inhibits growth of melanoma brain metastasis cell lines *in vitro*. Due to its small molecular size (422.46 Da) and hydrophobicity, HS-173 could be a promising candidate for subsequent animal studies, with the aim of bringing the drug into the clinic as an adjuvant treatment.

5.1 HS-173 effectively decreased cell viability

HS-173 inhibited cell viability in a dose-dependent manner in all four melanoma brain metastasis cell lines, even at doses as low as around 0.1 µM (**Fig. 4.1**). The viability curves were much steeper for the H2 and the H3 cells than the two other cell lines, indicating that incremental changes in concentration would have a larger inhibitory effect, which could explain the disparity in the IC_{50} doses (**Fig. 4.2**). The mean IC_{50} dose taking all cell lines into account was around 0.5 µM, and the lowest IC_{50} dose found was 0.15 µM for the H2 cell line, which is low compared to other studies[139,141,148].

Our monolayer viability results are in line with previous studies, which have shown the effectiveness of HS-173 (similar IC_{50} doses as ours) on other cancer cell lines, including squamous cell carcinoma, breast cancer, liver cancer and pancreatic cancer. Rumman and colleagues used an MTT assay on monolayers to show that pancreatic cancer cell lines had IC_{50} doses of around 1 µM[141].

Lee and colleagues tested the effects of HS-173 on liver cancer (HepG2, Huh7, Hep3B) and breast cancer (SkBr3, T47D, MCF-7) cell lines using an MTT assay. Both liver cancer and breast cancer had high rates of PI3Kα activating mutations, and the most sensitive cell line was HepG2 with an IC_{50} dose of only 0.045 µM, while the T47D showed lowest sensitivity at 0.4 µM[139]. It has been previously reported that HepG2 is a susceptible cell line to PI3Kα inhibition, and that T47D has an activating mutation in *PIK3CA*, which is the gene encoding PI3Kα[149,150].

It has also been shown that in pan-PI3K-resistant squamous cell carcinoma with *PIK3CA* activating mutations, HS-173 had a range of IC_{50} doses from under 1 µM to 25 µM[148].

Interestingly, although none of the cell lines tested in this thesis had *PIK3CA* activating mutations[151], their sensitivity to PI3Kα inhibition was still comparable to cancer cells harboring such mutations[151]. The cell lines used in this work have also previously been evaluated with the pan-PI3K inhibitor buparlisib, using the same protocol as in this thesis[121]. H1 and H2 cells were found to have around 2- to 8-fold lower IC_{50} doses using HS-173, compared to buparlisib treatment. The H3 cell line was found to be relatively resistant to buparlisib with an IC_{50} of around 20 µM, which is more than 10-fold higher than the IC_{50} of H3 to HS-173 (0.15 µM). On the contrary, H10 exhibited a higher IC_{50} to HS-173 when compared to buparlisib (1.0 µM compared to 0.43 µM). These results are corroborated by a high throughput screening study by Ryoo and colleagues aiming at investigating compounds suppressing miR-21 expression in the MDA-MB-231 breast cancer cell line. HS-173 was found to be a promising candidate, as the drug suppressed miR-21 expression more effectively compared to the pan PI3K inhibitors Wortmannin and LY294002, along with lower IC_{50} doses[152].

A possible explanation for the observed differences in IC_{50} doses may be that a larger amount of drug may be required in order to saturate and inhibit all PI3K isoforms, whereas the specificity of HS-173 means a lower concentration to fully inhibit the protein of interest. This is the reasoning behind introducing isoform-specific inhibitors in the clinic over pan-inhibitors, to reduce maximal doses and toxicity[153]. Additionally, pan-PI3K inhibitors may illicit a larger cellular response because they inhibit all forms of PI3K, which may trigger tumour cells to initiate resistance mechanisms more quickly.

These findings indicate that even without the activating *PIK3CA* mutation, HS-173 acted as an effective inhibitor of cell viability in all four melanoma cell lines. It functions as a more consistent growth inhibitor than the pan-PI3K inhibitor buparlisib in the same cells, decreasing cell growth in all cell lines including H3, a cell line which is resistant to buparlisib.

In order to substantiate the monolayer viability results, our initial plan was to perform viability studies in a 3D assay, by embedding the cells into soft agar. This is an assay which more closely mimics the environment *in vivo*, as the cells would be restricted by the agar and form spheroids, thus forming similar tumour structures as seen in patients[154]. Then, the idea was to treat the cells with similar dosages as used for the monolayer viability studies, over a time period for up to 14 days. Due to the coronavirus outbreak, the lab was closed, so there was

no time to carry on these experiments. In a previous study the PARP inhibitor PJ34 was found to inhibit the growth of H1 and H3 spheroids in a similar manner as seen in monolayer experiments[155]. Thus, it is likely that we would have observed similar, inhibitory effects using HS-173. We can of course not say whether treatment of 3D tumour structures with HS-173 would be as effective as monolayer treatment. However, it is worth mentioning that in previous studies treating H1 cells with memantine and thiostrepton, larger inhibitory effects were seen for both drugs on spheroids, compared to monolayers[156]. In contradiction, in Aasen and colleague's paper where H1, H2, H3 and H10 were tested with pan-PI3K inhibitor buparlisib, monotherapies were less effective in a 3D format[121]. This is a common result seen in 2D vs 3D culture systems, as in colonies cells tend to have more resistance to drug treatments because they more reflect the *in vivo* tumour environment.

5.2 HS-173 induces morphology changes in brain metastasis cell lines

In order to investigate potential morphological changes in cells over the course of treatment, light microscopy images were taken of each cell line after 72 hrs of treatment with increasing doses of HS-173. While each cell line had minor changes in morphological differences, the overall effect was similar. HS-173 induced a population of unattached, rounded cells as doses increased, and those that remained attached had reduced filopodia and spindles.

Rumman and colleagues found similar results on pancreatic cancer cell lines. In this study, migration was promoted through TGF-β exposure, and morphological changes upon treatment with HS-173 were assessed. TGF-β induced a mesenchymal phenotype in untreated cells, however those treated with 5 μM HS-173 had a more "cuboidal" shape with less filopodia[141]. Similar morphological changes were also reported during treatment with buparlisib by Aasen and colleagues[121].

The most likely explanation of the morphological change is by initiation of apoptosis in the cells. Apoptosis begins with a "rounding up" of cells, followed by blebbing of the surface membranes, and finally formation of fragmented apoptotic bodies[157]. This is especially notable in the H2 and H3 cell lines, where cell debris was present at the higher doses of HS-173 (**Fig. 4.3, 4.4**). H1 and H10 (**Fig. 4.2, 4.5**) cells did have smaller pieces of cell debris, but there were larger more rounded cells with no blebbing membranes. While this could indicate the initial stages of apoptosis, there is evidence that PI3K inhibition also may cause this type of morphology independent of apoptosis. In Aasen and colleague's paper, melanoma cells treated with buparlisib showed a circular morphology compared to untreated cells, however those same

cells treated with trametinib had an elongated morphology. Both these treated cells were found to be undergoing similar amounts of apoptosis, indicating that this morphology could be related specifically to PI3K pathway inhibition as well as apoptosis[121].

In a study by Wallin and colleagues, an invasive cell line was created from normal MCF10A, a non-tumourigenic human breast epithelial cell line, by knocking in an activating mutation in *PIK3CA*. It was found that the invasive cells developed a spindle-like, fibroblast morphology, and that this morphology was reversible when treated with PI3K inhibitors, both pan and isoform-specific[158]. Ryoo and colleagues also found that when their breast cancer cells were treated with HS-173, the cells exhibited a round shape. They speculated this could be due to the reversal of EMT transition through the reduction of miR-21 expression and upregulation of PTEN[152].

Overall, HS-173 induced morphological changes most likely attributed to apoptosis. However, the observed round phenotype has been seen in other studies evaluating the effect on the PI3K pathway in cancer and could implicate a cellular response other than apoptosis, related to metastasis and EMT transition[152,158]. Time restriction did not allow us to pursue this matter any further.

5.3 HS-173 reduces cell growth and migration in melanoma metastasis cell lines

The scratch wound assay showed that HS-173 reduced the capacity of the cells to close the wounds in a dose-dependent manner (**Fig. 4.6-4.9**). For all cell lines, the two highest doses effectively reduced cell migration. However, the H2 cell line where untreated controls did not have the ability to close the wound, seemed to be less affected by the anti-migrational effect of the drug.

Out of the four publications in which cells were treated with HS-173 and wound-healing assays were performed[139,141,152,159], all found that HS-173 reduced cell migration. In a study by Lee and colleagues, HUVEC cells were plated and migration was induced by the addition of VEGF, a growth factor often implicated in cancer metastases[139]. HS-173 was shown to reduce the migration of cells into the wound after 18 hrs. It should be noted that the doses used were much higher (10 µM and 50 µM) than those used in the 3 other papers, and also in this thesis. This increased dosage required to illicit a response in HUVECs, a non-tumourigenic cell line, is also an indication that HS-173 has a ‘therapeutic window’ in which tumour cells are affected but normal cells are not.

Rumman and colleagues performed a wound healing assay with pancreatic cancer lines and induced EMT-related migration by supplementing the media with TGF-β. They discovered that TGF-β-only treated cells migrated much faster than the untreated control, but those treated with both TGF-β and HS-173 reduced wound migration in a dose-dependent manner[141]. Ryoo and colleagues observed a more than 20% decrease in wound healing in their HS-173-treated breast cancer cell line[152]. In a study aiming to investigate the Wnt-5a activated migration of osteosarcoma cells, it was found that the cell lines exhibited a significantly reduced capacity of wound healing when treated with only 1 nM of HS-173. The authors concluded that PI3K acted as a downstream pathway from Wnt-5a to induce osteosarcoma migration and invasiveness[159].

Our results on cell migration may be explained by the following. We have already shown that viability decreases at the doses of HS-173 used in this work, and inhibited cell growth and apoptosis would prevent migration (**Fig. 4.1, Table 4.1**). On a molecular level, it has also been demonstrated that Wnt5a overexpression in melanoma cell lines increases melanoma invasion, and expression levels of Wnt5a in human melanoma biopsies correlates with increased tumour grade[160]. Wnt5a signaling has been related to increased p-Akt levels, and acts as a positive effector of migration in melanoma[161]. We have shown here that p-Akt is reduced upon treatment of HS-173 in our cells (to be explained further in **Section 5.5**), and this could explain the reduced migration we see across all cell lines. If this is the case, not only would HS-173 have the capacity to stop tumour growth, but also possibly inhibit further dissemination of metastases. Furthermore, as previously discussed in **Section 5.2**, if the phenotype change after HS-173 treatment is due to reversal of EMT, there would be a reduction in migration compared to the control, as cells typically become more mobile after undergoing EMT.

5.4 HS-173 induces apoptosis in melanoma metastasis cell lines

In order to find out if the morphological changes could be attributed to apoptosis, we performed an annexin V/PI assay using flow cytometry. Apoptotic cell populations were confirmed to increase in a dose-dependent manner, (**Fig. 4.11, 4.12**). H2 had a viability of roughly 70%, and H3 around 60% at doses 2-5 times higher than the IC_{50} which reflects numbers seen in the literature. H1 and H10 cells (**Fig. 4.10, 4.13**) had a comparatively larger amount of apoptosis in doses closer to the IC_{50}. H10 specifically had a very significant drop in

viable cells to around 40% at 1.0 µM, and a similar amount at 1.5 µM, while H1 had around 50% viable cells at 1.0 µM (**Fig. 4.14)**.

Overall, apoptotic numbers in H2 and H3 cells reflect those found in the literature, while H1 and H10 cells actually show more apoptosis after treatment than in most studies. Lee and colleagues found that upon treatment with 1.0 µM HS-173, Hep3B and SkBr3 cells both had significant increases in cells arrested in G_2/M phase, from 10-20% in control cells to 50-70% in treated cells. Treated cells were also around 30-40% positive in TUNEL assays compared to <10% in the controls[139]. These apoptotic numbers reflect what we found in some of our cell lines, although it should be noted these experiments were run with a 24 hrs time point. In the same study, a JC-1 assay quantifying mitochondrial stress found 20-30% cells undergoing apoptosis compared to 3-7% in the controls[139].

Yun and colleagues utilized TUNEL staining to quantify apoptosis in HS-173 treated Panc-1 pancreatic cancer cells, also using 1 µM for 24 hrs. Again, around 30-40% of cells were undergoing apoptosis, compared to the control at around 20%. HS-173 treatment also caused a very minor increase in G_2/M arrest, although there were no statistics performed[162].

Although our results are corroborated by the literature, we were hoping to further investigate the induction of apoptosis in our cells by HS-173. Most studies showed apoptosis at a 24 hrs time point, and with our 72 hrs time point, the cells may have been undergoing the entire apoptotic process and been completely destroyed. In the ungated samples with the highest concentration of drugs, the amount of debris gated out was higher (>10%) than in the control (data not shown). In the images taken of each condition, H2 cells (**Fig. 4.2**) and H3 cells (**Fig. 4.4**) had a large amount of cell debris, especially in the 0.5 µM sample. In addition, in the preparation of samples the cells were spun down at 400 x g and filtered. Larger apoptotic bodies can be pelleted at 400 x g but in experiments for isolating apoptotic bodies, samples are typically spun at 1000 to 4000 x g which would mean we are losing them in the sample preparation process[163]. Even if they were to be included however, debris cannot be counted in flow cytometry as each ‘event’ is representative of a single cell, and if debris is included results can be skewed.

Initially, we planned to test this hypothesis by performing the experiments again at 24 hrs timepoint instead of 72 hrs, so we could see more immediate effects of HS-173 on each cell line. Also, it would have been pertinent to investigate the cell cycle distribution with flow

cytometry as well. Unfortunately, due to the coronavirus shut-down these experiments could not be performed.

5.5 HS-173 downregulates activation of key proteins in the PI3K pathway

In all our cell lines, the main effect of HS-173 treatment was a reduction in Akt phosphorylation at Ser^{473}. The timeline of effects varied between cell lines, with H1 having the main effect at 24 hrs (**Fig. 4.15**) and 48 hrs and H2 at 72 hrs (**Fig. 4.16**). Unfortunately, due to time constraints, it was not possible to get all three timepoints for the H3 cells, but the effect of HS-173 was still visible after 72 hrs (**Fig. 4.17**). In **Fig. 4.18**, H10 had an immediate response to HS-173, and p-Akt expression was lowest at 24 hrs and recovered across the next two days.

There are several studies presenting the same effect of HS-173 on p-Akt expression[139,142,143,148,162,164]. Jung and colleagues tested HS-173 in overactive fibroblast plaque tissue from patients with Peyronie's disease. At a dose of 5 µM administered for 24 hrs, the cells had almost no expression of p-Akt, compared to the control samples[164]. Lee and collaborators studied the Akt phosphorylation sites $Thre^{308}$ and Ser^{473} in liver cancer and breast cancer cell lines after 24 hrs of treatment with 0.1 µM, 0.5 µM and 1.0 µM of HS-173. Both cell lines had reduced p-Akt expression levels after being exposed to 0.5 µM, most notably at the Ser^{473} site[139]. Michmerhuizen and colleagues used a dose of 5 µM HS-1173 on six squamous cell carcinoma cell lines and in all of them, an inhibitory effect was shown in Akt phosphorylation[148].

Miapaca-2 and PANC-1 cells were studied by Yun and colleagues in a single treatment experiment, where they determined that 1 µM of HS-173 was sufficient to almost completely inhibit p-Akt expression[162]. These same cells were utilized to evaluate the ability for HS-173 to inhibit p-Akt in experiments where p-Akt was previously upregulated by using radiation. Park and co-workers studied the effect of HS-173 on irradiated pancreatic cancer cell lines (Miapaca-2 and PANC-1). Cells that were irradiated with 10 Gy had a significant increase in p-Akt levels, and HS-173 was able to reduce the expression of p-Akt below the control sample levels and 10 Gy irradiated samples in doses from 1 - 5 µM of HS-173[142].

Overall, it seemed as though phosphorylation of mTOR was not largely affected by HS-173 at the doses used in this work. Some minor changes were seen, particularly in H1 cells at 48 hrs (**Fig. 4.15**), and H2 cells at 72 hrs. Since these experiments were only carried through once due to time limitations, a quantification could not be performed as this requires minimum

3 independent experiments. In the literature, mTOR activation is found to be less affected by HS-173 than Akt activation, although activation inhibition could be seen in higher doses, and in shorter time points[139,164].

Jung and colleagues also found that mTOR phosphorylation was reduced by HS-173, but not to the degree in which p-Akt was affected and requiring almost 4 times the dose (20 μM) to cause a large decrease in expression. It is worth noting that they also performed immunocytochemistry (ICC) on the cells after only a 6 hrs exposure, and p-mTOR had a much larger decrease in expression at this timepoint at only 1 μM, suggesting that the activation of mTOR is affected, but recovers very quickly[164]. Lee and colleagues also found very similar results in their liver and breast cancer cell lines, that inhibition of mTOR phosphorylation required a higher dose than in p-Akt, and that in ICC with a short exposure time (2 hrs), p-mTOR expression was barely visible[139].

It is possible that mTOR recovers more quickly as it is further downstream from the protein being inhibited, resulting in higher probability for compensation mechanisms from other effectors. Additionally, mTOR protein forms two major complexes in the cell (mTORC1 and mTORC2), one downstream from Akt and one upstream. A larger amount of inhibition may be required before a significant decrease can be detected through western blotting. Although Akt does have some PI3K-independent methods of activation, the major mechanism occurs directly from PI3K catalysis of second messenger PIP_3. A known mechanism in cancer, found in melanoma specifically, for mTOR reactivation in response to PI3K pathway inhibition is downregulation of mTOR inhibitor TSC2, which has been proven to increase the activation of mTOR. TSC2 is inactivated by phosphorylation, and the kinases involved have been documented to play a role in PI3K inhibitor resistance[165].

Similar to p-mTOR, PI3Kα had minor changes in the treated samples versus the control. In all cell lines, at least one time point showed a slight decrease in PI3Kα, H1 (**Fig. 4.15**) at 48 hrs, H2 (**Fig. 4.16**) at 72 hrs, H3 (**Fig. 4.17**) at 72 hrs, and H10 (**Fig. 4.18**) at 24 and 48 hrs.

No previous studies have assessed the effects of PI3Kα expression after HS-173 treatment. Thus, it is not possible to relate our findings to any published work with isoform-specific inhibition, however there are some publications evaluating pan-PI3K inhibition and PI3K expression. Aasen and colleagues studied buparlisib and trametinib on metastatic melanoma cell lines, and found that PI3K was reduced in the presence of buparlisib, equally as much as when treated with both drugs in combination[121]. Luo and colleagues investigated the

effect of two PI3K inhibitors, wortmannin and LY294002 in a laryngeal carcinoma xenograft mouse model. During single treatments with each inhibitor, tumour cells were found to have a significantly reduced amount of PI3K expression compared to the control[166].

In summary, HS-173 downregulated the expression levels of p-Akt, a major regulator in the PI3K pathway. Additionally, there were some indications that activation of p-mTOR and the expression of PI3Kα was altered after HS-173 treatment, although not to the degree of p-Akt. Based on previous research, it is reasonable that with PI3Kα inhibition there would be reduction in its own expression. The PI3K pathway in melanoma is thought to have self-promoting feedback loops and inhibiting the pathway could alter expression of the protein itself[167]. Unfortunately, due to time constraints we could not perform triplicate experiments with quantifications to reliably verify these findings.

5.6 Experimental Limitations and Considerations

There are several things that should be taken into consideration in terms of HS-173 as a possible therapeutic agent. A major issue with targeted therapies is acquired resistance to the drug being used. Melanoma has several mechanisms to adjust signaling in response to pathway inhibition as previously discussed, and therefore monotherapies are rarely very effective in patients for very long. In the case of HS-173, the target of interest is isoform-specific and therefore allows the possibility for cells of isoform switching. However, combined therapy is likely required to inhibit the upregulated PI3K pathway at several levels, in addition to other pathways that could be activated in response to treatment (i.e. MAPK). In this case, the HS-173 specificity and low effective doses could be beneficial.

HS-173 has been shown in several studies to work in combination with other inhibitors in a synergistic fashion. HS-173 enhanced the efficacy and penetration of doxorubicin into MIA PaCa-2 and B16 tumours *in vivo*[140] and displayed potential synergy with gefitinib (EGFR inhibitor) in advanced stage head and neck squamous cell carcinoma[143]. A synergistic anticancer effect was also induced by HS-173 in combination with sorafenib (multi-kinase inhibitor in MAPK pathway) in pancreatic cells. Although these results cannot definitively predict that HS-173 will always work in a synergistic function when combined with other drugs, it is promising that it does so with inhibitors of the MAPK pathway.

It has been shown that in *BRAF*-mutant melanoma, PI3K pathway inhibitors can be effective in tumours without major *PI3K* pathway mutations[136]. Nevertheless, determining the mutations that cause the sensitivity to this inhibitor is important for personalized therapies in

the future. Although it is impossible to say which specific mutations are relevant in this thesis without further experimentation, a previous mutational analysis was considered in order to begin investigating the possible explanation.

There are several mutations previously found in melanoma that can activate the PI3K pathway. Mutations in RTKs, which activate PI3K at the very beginning of the pathway, can increase the activity of the pathway. RTK mutations have been found in up to 49% of cutaneous melanomas, and mutations directly within the PI3K pathway have been found in 56%[40]. H1 and H10 both have mutations in the *FGFR2* gene, and H10 has a mutation in both *EGFR* and *PDGFRB* genes, all of which are RTKs that can activate the PI3K pathway[151]. TSC1, an inhibitory effector to mTOR, is also mutated in H1. Inactivating mutations in TSC1, like PTEN, can lead to PI3K pathway activation. *NRAS*, which codes for the NRAS protein in the MAPK pathway, has also been found to stimulate PI3Kα activation[151]. Additionally, it has been speculated that the PI3K pathway plays an important role in mediating BRAF inhibitor resistance, suggesting that melanoma tumours have the ability to upregulate the PI3K pathway upon induced resistance to MAPK pathway targeted treatments although the mechanisms behind this requires more investigation[168].

A major obstacle in treatment of melanoma brain metastases is to deliver drugs across the blood brain barrier. There have been no studies so far showing that HS-173 can penetrate through the brain microvasculature, although the molecular characteristics are promising. It is a small molecule at only 422.46 Da, in addition to being lipid soluble and therefore has the potential to be able to cross the BBB. Furthermore, the BBB tends to lose the integrity in the presence of a tumour, additionally facilitating the possibility of HS-173 to be utilized to treat brain metastases[169].

In this thesis, we studied the *in vitro* effects of HS-173. The drug has also shown promising effects *in vivo*. In a xenograft model with PANC-1 and Miapaca-2 pancreatic cancer cell lines, HS-173 was found to reduce tumour growth and sensitize the tumours to radiotherapy at a dose of 10 mg/kg, 5 times/week for four weeks[142]. Rumman and colleagues utilized three pancreatic mouse cancer models: a xenograft model, an orthotopic model and a metastasis model to liver, lung and lymph nodes. In xenograft and orthotopic models, mice were treated with 10 mg/kg. Significant reduction in tumour sizes were observed, while no major changes in body weight and no adverse effects were noted[141]. The metastatic model was treated with either 10 mg/kg or 30 mg/kg three times a week for 25 days and resulted in significant reductions in lung and liver metastases at both doses.

Moving forward it is important to evaluate HS-173 in our own *in vivo* brain metastasis mouse models, to be discussed further in **Future Aspects**.

Conclusion

Overall, the results of this study support previous literature showing anti-cancer effects of HS-173. The drug inhibited cell viability and induced apoptosis in a dose-dependent manner. All cell lines showed rounded morphological changes after treatment, which may be attributed to apoptosis, and this could also indicate a reduction in Akt dependent-EMT potential. Proliferation and migration were reduced in the presence of HS-173, as shown by a wound-healing assay. Western blots demonstrated that the PI3K signaling pathway was affected, with major reductions in Akt protein expression levels, and minor changes in expression levels of mTOR and PI3Kα.

In conclusion, we demonstrate for the first time that the PI3Kα inhibitor HS-173 effectively inhibits the growth of human melanoma brain metastasis cell lines *in vitro*. The promising results should be followed up with further studies, to determine its potential applicability in the clinic.

Future Aspects

To establish the use of HS-173 as a therapeutic option in the treatment of melanoma brain metastasis, several additional experiments need to be performed.

HS-173 was effective in monolayer cultures, however these assays do not reflect the three-dimensional (3D) growth seen clinically. Thus; 3D *in vitro* assays such as the soft agar assay should be performed to establish that the drug also is effective in a clinically more relevant situation. We started on these experiments, but they are considerably more time-consuming than monolayer assays, and we had to discard the culture plates when the lab was closed in March.

Due to time constraints, we were not able to verify the western blots in triplicate experiments, so this should be repeated on the signaling proteins studied in this thesis. Also, the drug doses should be increased, to establish that the drug inhibits protein levels such as p-mTOR and PI3Ka, which were only modestly affected in this study. Previous literature has shown reduced expression levels of these proteins, using higher doses.

The effects of HS-173 on caspases could also be evaluated with western blotting to corroborate the apoptosis data gathered from flow cytometry.

Further, the effects on signaling proteins in the PI3K signaling pathway, such as BAD, CREB or FOXO should be evaluated by western blots. Also, potential crosstalk between the PI3K and the MAPK signaling pathways could be elucidated by blotting expression levels of MAPK proteins after drug exposure. Expression of E-cadherin and N-cadherin could also be investigated to elucidate if the morphology change of the cells is related to EMT reversal.

We show that HS-173 induces apoptosis to a certain degree. In this respect, it may well be that drug treatment also induces for instance cell cycle arrest, which could easily be studied by flow cytometry. Time limitations did not allow us to follow up on this.

Prior to moving into preclinical experiments, a therapeutic window for the drug has to be established. Thus, HS-173 should also be tested on healthy, non-tumourigenic cells such as brain astrocytes and endothelial cells to confirm that HS-173 will not induce cell death at the same doses as for the tumour cells. There is already an indication that non-tumourigenic cell lines (HUVECS) are less sensitive to HS-173, as discussed in **Section 5.3**.

In vivo, the ability of HS-173 to penetrate an intact blood-brain barrier should be firmly established. This can be done by radiolabeling the drug with ^{11}C, and then performing dynamic PET studies in non-tumour bearing animals. This is a feasible project, since the group has already established collaborations with Radiochemists at the PET Center (Haukeland University Hospital) and Medical Chemists at the Department of Chemistry, UiB.

Next, animal treatment studies should be performed, using our well-established animal/tumour models. Human melanoma brain metastasis cells are injected intracardially into nod/scid mice, and brain metastasis development are monitored by MRI and PET/CT. Clinically relevant doses of HS-173 should be administered to the mice, and effects on tumour burden and animal survival should be recorded. Alpelisib, a PI3Kα inhibitor that has been shown not to cross the BBB, has been used in mouse models in doses of 12.5, 25 or 50 mg/kg, which could be used as a starting point for dose selection for effective treatment with HS-173[170]. Further, the pan-PI3K inhibitor buparlisib has previously been administered to mice at a dose of 50 mg/kg, and based on our discussion of *in vitro* doses necessary for tumour cell inhibition (Section 5.1), this suggests that HS-173 may be effective in animal studies even at lower doses[121].

Also, subsequent histology and immunohistochemistry would reveal changes in tumour morphology and expression levels of relevant signaling proteins.

References

1. Katalinic A, Kunze U, Schäfer T. Epidemiology of cutaneous melanoma and non-melanoma skin cancer in Schleswig-Holstein, Germany: incidence, clinical subtypes, tumour stages and localization (epidemiology of skin cancer). *Br J Dermatol*. 2003;149(6):1200-1206. https://doi.org/10.1111/j.1365-2133.2003.05554.x
2. Apalla Z, Lallas A, Sotiriou E, Lazaridou E, Ioannides D. Epidemiological trends in skin cancer. *Dermatol Pract Concept*. 2017;7(2):1-6. https://doi.org/10.5826/dpc.0702a01
3. Nelson TG, Ashton RE. Low incidence of metastasis and recurrence from cutaneous squamous cell carcinoma found in a UK population: Do we need to adjust our thinking on this rare but potentially fatal event? *J Surg Oncol*. 2017;116(6):783-788.
4. Bliss D. *Layers of the Skin*. National Cancer Institute; 2005.
5. American Cancer Society. Cancer Facts and Figures 2018. Atlanta: American Cancer Society; 2019.
6. Bray F, Ferlay J, Soerjomataram I, Siegel RL, Torre LA, Jemal A. Global cancer statistics 2018: GLOBOCAN estimates of incidence and mortality worldwide for 36 cancers in 185 countries. *CA Cancer J Clin*. 2018;68(6):394-424. https://doi.org/10.3322/caac.21492
7. Robsahm TE JT, Bachmann IM. Nasjonale retningslinjer for diagnostikk, behandling og oppfølging av maligne melanomer. Oslo: Helsedirektoratet; 2011.
8. Robsahm TE, Bergva G, Hestvik UE, Møller B. Sex differences in rising trends of cutaneous malignant melanoma in Norway, 1954-2008. *Melanoma Res*. 2013;23(1):70-78. https://doi.org/10.1097/CMR.0b013e32835c7e48
9. Veierød MB. Forekomsten av føflekkreft øker igjen. *Tidsskr Nor Legeforen*. 2015;135(5):450-452. https://doi.org/10.4045/tidsskr.14.1109
10. Yuan T-A, Lu Y, Edwards K, Jakowatz J, Meyskens FL, Liu-Smith F. Race-, age-, and anatomic site-specific gender differences in cutaneous melanoma suggest differential mechanisms of early- and late-onset melanoma. *Int J Environ Res Public Health*. 2019;16(6):908. https://doi.org/10.3390/ijerph16060908
11. Ward-Peterson M, Acuña JM, Alkhalifah MK, et al. Association between race/ethnicity and survival of melanoma patients in the United States over 3 decades: a secondary analysis of SEER data. *Medicine (Baltimore)*. 2016;95(17):e3315. https://doi.org/10.1097/MD.0000000000003315
12. Matthews NH, Li W-Q, Qureshi AA, Weinstock MA, Cho E. Epidemiology of melanoma. In: Ward WH, Farma JM, ed. *Cutaneous Melanoma: Etiology and Therapy*. Singapore: Codon Publications; 2017. https://doi.org/10.15586/codon.cutaneousmelanoma.2017.ch1
13. Jiang AJ, Rambhatla PV, Eide MJ. Socioeconomic and lifestyle factors and melanoma: a systematic review. *Br J Dermatol*. 2015;172(4):885-915. https://doi.org/10.1111/bjd.13500
14. Robsahm TE, Helsing P, Nilssen Y, et al. High mortality due to cutaneous melanoma in Norway: a study of prognostic factors in a nationwide cancer registry. *Clin Epidemiol*. 2018;10:537-548. https://doi.org/10.2147/CLEP.S151246
15. Wu S, Zhu W, Thompson P, Hannun YA. Evaluating intrinsic and non-intrinsic cancer risk factors. *Nat Commun*. 2018;9(1):3490. https://doi.org/10.1038/s41467-018-05467-z
16. Gordon R. Skin cancer: an overview of epidemiology and risk factors. *Semin Oncol Nurs*. 2013;29(3):160-169. https://doi.org/10.1016/j.soncn.2013.06.002
17. Elwood JM, Jopson J. Melanoma and sun exposure: an overview of published studies. *Int J Cancer*. 1997;73(2):198-203. https://doi.org/10.1002/(SICI)1097-0215(19971009)73:23.0.CO;2-R
18. Rastrelli M, Tropea S, Rossi CR, Alaibac M. Melanoma: epidemiology, risk factors, pathogenesis, diagnosis and classification. *In Vivo*. 2014;28(6):1005-1011.
19. International Union Against Cancer. The association of use of sunbeds with cutaneous malignant melanoma and other skin cancers: a systematic review. *Int J Cancer*. 2006;120(5):1116-1122.
20. Stern RS. The risk of melanoma in association with long-term exposure to PUVA. *J Am Acad Dermatol*. 2001;44(5):755-761. https://doi.org/10.1067/mjd.2001.114576
21. Diffey BL. Stratospheric ozone depletion and the risk of non-melanoma skin cancer in a British population. *Phys Med Biol*. 1992;37(12):2267. https://doi.org/10.1088/0031-9155/37/12/008

22. Martens WJM, den Elzen MGJ, Slaper H, Koken PJM, Willems BAT. The impact of ozone depletion on skin cancer incidence: an assessment of the Netherlands and Australia. *Environ Model Assess*. 1996;1(4):229-240. https://doi.org/10.1007/BF01872152
23. World Health Organization. *Climate change and human health: risks and responses*. World Health Organization; 2003.
24. Volkovova K, Bilanicova D, Bartonova A, Letašiová S, Dusinska M. Associations between environmental factors and incidence of cutaneous melanoma. Review. *Environ Health*. 2012;11(Suppl. 1):S12. https://doi.org/10.1186/1476-069X-11-S1-S12
25. Orthaber K, Pristovnik M, Skok K, Perić B, Maver U. Skin cancer and its treatment: novel treatment approaches with emphasis on nanotechnology. *J Nanomater*. 2017;2017: 2606271. https://doi.org/10.1155/2017/2606271
26. Gandini S, Sera F, Cattaruzza MS, et al. Meta-analysis of risk factors for cutaneous melanoma: I. Common and atypical naevi. *Eur J Cancer*. 2005;41(1):28-44. https://doi.org/10.1016/j.ejca.2004.10.015
27. Goldstein AM, Tucker MA. Dysplastic nevi and melanoma. *Cancer Epidemiol Biomarkers Prev*. 2013;22(4):528-532. https://doi.org/10.1158/1055-9965.EPI-12-1346
28. Tsao H, Niendorf K. Genetic testing in hereditary melanoma. *J Am Acad Dermatol*. 2004;51(5):803-808. https://doi.org/10.1016/j.jaad.2004.04.045
29. de Snoo FA, Bishop DT, Bergman W, et al. Increased risk of cancer other than melanoma in CDKN2A founder mutation (p16-Leiden)-positive melanoma families. *Clin Cancer Res*. 2008;14(21):7151-7157. https://doi.org/10.1158/1078-0432.CCR-08-0403
30. Helsing P, Nymoen DA, Ariansen S, et al. Population-based prevalence of *CDKN2A* and *CDK4* mutations in patients with multiple primary melanomas. *Genes Chromosomes Cancer*. 2008;47(2):175-184.
31. Mort RL, Jackson IJ, Patton EE. The melanocyte lineage in development and disease. *Development*. 2015;142(4):620-632. https://doi.org/10.1242/dev.106567
32. DeVita VT, Lawrence TS, Rosenberg SA. *Cancer: Principles & Practice of Oncology: Primer of the molecular biology of cancer*. Philadelphia: Wolters Kluwer Health; 2015.
33. Sturm RA, Box NF, Ramsay MJB. Human pigmentation genetics: the difference is only skin deep. *Bioessays*. 1998;20(9):712-721. https://doi.org/10.1002/(SICI)1521-1878(199809)20:93.0.CO;2-I
34. Kaidbey KH, Agin PP, Sayre RM, Kligman AM. Photoprotection by melanin—a comparison of black and Caucasian skin. *J Am Acad Dermatol*. 1979;1(3):249-260. https://doi.org/10.1016/S0190-9622(79)70018-1
35. Bustamante J, Bredeston L, Malanga G, Mordoh J. Role of melanin as a scavenger of active oxygen species. *Pigment Cell Res*. 1993;6(5):348-353. https://doi.org/10.1111/j.1600-0749.1993.tb00612.x
36. Lawrence MS, Stojanov P, Polak P, et al. Mutational heterogeneity in cancer and the search for new cancer-associated genes. *Nature*. 2013;499(7457):214-218. https://doi.org/10.1038/nature12213
37. Karachaliou N, Pilotto S, Teixidó C, et al. Melanoma: oncogenic drivers and the immune system. *Ann Transl Med*. 2015;3(18):265.
38. Colombino M, Capone M, Lissia A, et al. BRAF/NRAS mutation frequencies among primary tumors and metastases in patients with melanoma. *J Clin Oncol*. 2012;30(20):2522-2529. https://doi.org/10.1200/JCO.2011.41.2452
39. Curtin JA, Fridlyand J, Kageshita T, et al. Distinct sets of genetic alterations in melanoma. *N Engl J Med*. 2005;353(20):2135-2147. https://doi.org/10.1056/NEJMoa050092
40. Hayward NK, Wilmott JS, Waddell N, et al. Whole-genome landscapes of major melanoma subtypes. *Nature*. 2017;545(7653):175-180. https://doi.org/10.1038/nature22071
41. Daum G, Eisenmann-Tappe I, Fries HW, Troppmair J, Rapp UR. The ins and outs of Raf kinases. *Trends Biochem Sci*. 1994;19(11):474-480. https://doi.org/10.1016/0968-0004(94)90133-3
42. Wellbrock C, Karasarides M, Marais R. The RAF proteins take centre stage. *Nat Rev Mol Cell Biol*. 2004;5(11):875-885. https://doi.org/10.1038/nrm1498
43. Niault TS, Baccarini M. Targets of Raf in tumorigenesis. *Carcinogenesis*. 2010;31(7):1165-1174. https://doi.org/10.1093/carcin/bgp337

44. Davies H, Bignell GR, Cox C, et al. Mutations of the BRAF gene in human cancer. *Nature*. 2002;417(6892):949-954. https://doi.org/10.1038/nature00766
45. Lokhandwala PM, Tseng L-H, Rodriguez E, et al. Clinical mutational profiling and categorization of BRAF mutations in melanomas using next generation sequencing. *BMC Cancer*. 2019;19(1):665. https://doi.org/10.1186/s12885-019-5864-1
46. Ihle MA, Fassunke J, König K, et al. Comparison of high resolution melting analysis, pyrosequencing, next generation sequencing and immunohistochemistry to conventional Sanger sequencing for the detection of p. V600E and non-p. V600E BRAF mutations. *BMC Cancer*. 2014;14(1):13. https://doi.org/10.1186/1471-2407-14-13
47. Ribas A, Flaherty KT. BRAF targeted therapy changes the treatment paradigm in melanoma. *Nat Rev Clin Oncol*. 2011;8(7):426-433. https://doi.org/10.1038/nrclinonc.2011.69
48. Carlino MS, Haydu LE, Kakavand H, et al. Correlation of BRAF and NRAS mutation status with outcome, site of distant metastasis and response to chemotherapy in metastatic melanoma. *Br J Cancer*. 2014;111(2):292-299. https://doi.org/10.1038/bjc.2014.287
49. Diaz-Flores E, Shannon K. Targeting oncogenic Ras. *Genes Dev*. 2007;21(16):1989-1992. https://doi.org/10.1101/gad.1587907
50. Hodis E, Watson IR, Kryukov GV, et al. A landscape of driver mutations in melanoma. *Cell*. 2012;150(2):251-263. https://doi.org/10.1016/j.cell.2012.06.024
51. Hobbs GA, Der CJ, Rossman KL. RAS isoforms and mutations in cancer at a glance. *J Cell Sci*. 2016;129(7):1287-1292. https://doi.org/10.1242/jcs.182873
52. Li A, Ma Y, Jin M, et al. Activated mutant NRas(Q61K) drives aberrant melanocyte signaling, survival, and invasiveness via a Rac1-dependent mechanism. *J Invest Dermatol*. 2012;132(11):2610-2621. https://doi.org/10.1038/jid.2012.186
53. Muñoz-Couselo E, Adelantado EZ, Ortiz C, García JS, Perez-Garcia J. NRAS-mutant melanoma: current challenges and future prospect. *Onco Targets Ther*. 2017;10:3941-3947. https://doi.org/10.2147/OTT.S117121
54. Prior IA, Lewis PD, Mattos C. A comprehensive survey of Ras mutations in cancer. *Cancer Res*. 2012;72(10):2457-2467. https://doi.org/10.1158/0008-5472.CAN-11-2612
55. Burd CE, Liu W, Huynh MV, et al. Mutation-specific RAS oncogenicity explains NRAS codon 61 selection in melanoma. *Cancer Discov*. 2014;4(12):1418-1429. https://doi.org/10.1158/2159-8290.CD-14-0729
56. Adler NR, Haydon A, McLean CA, Kelly JW, Mar VJ. Metastatic pathways in patients with cutaneous melanoma. *Pigment Cell Melanoma Res*. 2017;30(1):13-27. https://doi.org/10.1111/pcmr.12544
57. Mar VJ, Wong SQ, Li J, et al. BRAF/NRAS wild-type melanomas have a high mutation load correlating with histologic and molecular signatures of UV damage. *Clin Cancer Res*. 2013;19(17):4589-4598. https://doi.org/10.1158/1078-0432.CCR-13-0398
58. Cancer Genome Atlas Network. Genomic classification of cutaneous melanoma. *Cell*. 2015;161(7):1681-1696. https://doi.org/10.1016/j.cell.2015.05.044
59. Scheffzek K, Welti S. Neurofibromin: Protein Domains and Functional Characteristics. In: Upadhyaya M, Cooper DN, eds. *Neurofibromatosis Type 1: Molecular and Cellular Biology*. Berlin, Heidelberg: Springer Berlin Heidelberg; 2012:305-326. https://doi.org/10.1007/978-3-642-32864-0_20
60. Chu EC, Tarnawski AS. PTEN regulatory functions in tumor suppression and cell biology. *Med Sci Monit*. 2004;10(10):RA235-RA241.
61. Tsao H, Zhang X, Benoit E, Haluska FG. Identification of PTEN/MMAC1 alterations in uncultured melanomas and melanoma cell lines. *Oncogene*. 1998;16(26):3397-3402. https://doi.org/10.1038/sj.onc.1201881
62. Vogelstein B, Sur S, Prives C. p53: the most frequently altered gene in human cancers. *Nature Education*. 2010;3(9):6.
63. Martincorena I, Campbell PJ. Somatic mutation in cancer and normal cells. *Science*. 2015;349(6255):1483-1489. https://doi.org/10.1126/science.aab4082
64. Rabbie R, Ferguson P, Molina-Aguilar C, Adams DJ, Robles-Espinoza CD. Melanoma subtypes: genomic profiles, prognostic molecular markers and therapeutic possibilities. *J Pathol*. 2019;247(5):539-551. https://doi.org/10.1002/path.5213

65. University of Texas. Cancer Grade vs. Cancer Stage. MD Anderson Cancer Center. https://www.mdanderson.org/patients-family/diagnosis-treatment/a-new-diagnosis/cancer-grade-vs--cancer-stage.html. Accessed May 28, 2020.
66. Balch CM, Gershenwald JE, Soong S, et al. Final version of 2009 AJCC melanoma staging and classification. *J Clin Oncol*. 2009;27(36):6199-6206. https://doi.org/10.1200/JCO.2009.23.4799
67. Gershenwald JE, Scolyer RA. Melanoma staging: American Joint Committee on Cancer (AJCC) and beyond. *Ann Surg Oncol*. 2018;25(8):2105-2110. https://doi.org/10.1245/s10434-018-6513-7
68. Seyfried TN, Huysentruyt LC. On the origin of cancer metastasis. *Crit Rev Oncog*. 2013;18(1-2):43-73. https://doi.org/10.1615/CritRevOncog.v18.i1-2.40
69. Tas F. Metastatic behavior in melanoma: timing, pattern, survival, and influencing factors. J Oncol. 2012;2012:647684. https://doi.org/10.1155/2012/647684
70. Valastyan S, Weinberg RA. Tumor metastasis: molecular insights and evolving paradigms. *Cell*. 2011;147(2):275-292. https://doi.org/10.1016/j.cell.2011.09.024
71. Roche J. The epithelial-to-mesenchymal transition in cancer. *Cancers*. 2018;10(2):52. https://doi.org/10.3390/cancers10020052
72. Chiang SP, Cabrera RM, Segall JE. Tumor cell intravasation. *Am J Physiol Cell Physiol*. 2016;311(1):C1-C14. https://doi.org/10.1152/ajpcell.00238.2015
73. Guo W, Giancotti FG. Integrin signalling during tumour progression. *Nat Rev Mol Cell Biol*. 2004;5(10):816-826. https://doi.org/10.1038/nrm1490
74. Stelzer KJ. Epidemiology and prognosis of brain metastases. *Surg Neurol Int*. 2013;4(Suppl. 4):S192-S202. https://doi.org/10.4103/2152-7806.111296
75. Gavrilovic IT, Posner JB. Brain metastases: epidemiology and pathophysiology. *J Neurooncol*. 2005;75(1):5-14. https://doi.org/10.1007/s11060-004-8093-6
76. Nayak L, Lee EQ, Wen PY. Epidemiology of brain metastases. *Curr Oncol Rep*. 2012;14(1):48-54. https://doi.org/10.1007/s11912-011-0203-y
77. Nussbaum ES, Djalilian HR, Cho KH, Hall WA. Brain metastases: Histology, multiplicity, surgery, and survival. *Cancer*. 1996;78(8):1781-1788. https://doi.org/10.1002/(SICI)1097-0142(19961015)78:83.0.CO;2-U
78. Stark A, Stöhring C, Hedderich J, Held-Feindt J, Mehdorn H. Surgical treatment for brain metastases: prognostic factors and survival in 309 patients with regard to patient age. *J Clin Neurosci*. 2011;18(1):34-38. https://doi.org/10.1016/j.jocn.2010.03.046
79. Patel JK, Didolkar MS, Pickren JW, Moore RH. Metastatic pattern of malignant melanoma: A study of 216 autopsy cases. *Am J Surg*. 1978;135(6):807-810. https://doi.org/10.1016/0002-9610(78)90171-X
80. Zakrzewski J, Geraghty LN, Rose AE, et al. Clinical variables and primary tumor characteristics predictive of the development of melanoma brain metastases and post-brain metastases survival. *Cancer*. 2011;117(8):1711-1720. https://doi.org/10.1002/cncr.25643
81. Damsky WE Jr, Rosenbaum LE, Bosenberg M. Decoding melanoma metastasis. *Cancers (Basel)*. 2011;3(1):126-163. https://doi.org/10.3390/cancers3010126
82. Morgan SS, Jeter JM, Hersh EM, Yi SK, Cranmer LD. Management of Brain Metastasis in Melanoma Patients. In: Duc, GHT, ed. *Melanoma: From Early Detection to Treatment*. Norderstedt, Germany: Books on Demand; 2013.
83. Sampson JH, Carter JH, Friedman AH, Seigler HF. Demographics, prognosis, and therapy in 702 patients with brain metastases from malignant melanoma. *J Neurosurg*. 1998;88(1):11-20. https://doi.org/10.3171/jns.1998.88.1.0011
84. Gaudy-Marqueste C, Dussouil A, Carron R, et al. Survival of melanoma patients treated with targeted therapy and immunotherapy after systematic upfront control of brain metastases by radiosurgery. *Eur J Cancer*. 2017;84:44-54. https://doi.org/10.1016/j.ejca.2017.07.017
85. Sloot S, Chen YA, Zhao X, et al. Improved survival of patients with melanoma brain metastases in the era of targeted BRAF and immune checkpoint therapies. *Cancer*. 2018;124(2):297-305. https://doi.org/10.1002/cncr.30946
86. Pardridge WM. The blood-brain barrier: bottleneck in brain drug development. *NeuroRx*. 2005;2(1):3-14. https://doi.org/10.1602/neurorx.2.1.3
87. Abbott NJ, Patabendige AAK, Dolman DEM, Yusof SR, Begley DJ. Structure and function of the blood–brain barrier. *Neurobiol Dis*. 2010;37(1):13-25. https://doi.org/10.1016/j.nbd.2009.07.030

88. Daneman R, Prat A. The blood-brain barrier. *Cold Spring Harb Perspect Biol*. 2015;7(1):a020412. https://doi.org/10.1101/cshperspect.a020412
89. Banks WA. Characteristics of compounds that cross the blood-brain barrier. *BMC Neurol*. 2009;9(Suppl. 1):S3. https://doi.org/10.1186/1471-2377-9-S1-S3
90. Goyal S, Silk AW, Tian S, et al. Clinical management of multiple melanoma brain metastases: a systematic review. *JAMA Oncol*. 2015;1(5):668-676. https://doi.org/10.1001/jamaoncol.2015.1206
91. Glitza Oliva I, Tawbi H, Davies MA. Melanoma brain metastases: current areas of investigation and future directions. *Cancer J*. 2017;23(1):68-74. https://doi.org/10.1097/PPO.0000000000000237
92. Sturdza A, Millar B-A, Bana N, et al. The use and toxicity of steroids in the management of patients with brain metastases. *Support Care Cancer*. 2008;16(9):1041-1048. https://doi.org/10.1007/s00520-007-0395-8
93. Radiological Society of North America. Stereotactic Radiosurgery (SRS) and Stereotactic Body Radiotherapy (SBRT). https://www.radiologyinfo.org/en/info.cfm?pg=stereotactic. May 28, 2019. Accessed May 28, 2020.
94. Mizuno T, Takada K, Hasegawa T, et al. Comparison between stereotactic radiosurgery and whole-brain radiotherapy for 10-20 brain metastases from non-small cell lung cancer. *Mol Clin Oncol*. 2019;10(5):560-566. https://doi.org/10.3892/mco.2019.1830
95. Glitza Oliva I, Schvartsman G, Tawbi H. Advances in the systemic treatment of melanoma brain metastases. Ann Oncol. 2018;29(7):1509-1520.
96. Fetcko K, Lukas RV, Watson GA, Zhang L, Dey M. Survival and complications of stereotactic radiosurgery: a systematic review of stereotactic radiosurgery for newly diagnosed and recurrent high-grade gliomas. *Medicine (Baltimore)*. 2017;96(43):e8293. https://doi.org/10.1097/MD.0000000000008293
97. Vellayappan B, Tan CL, Yong C, et al. Diagnosis and management of radiation necrosis in patients with brain metastases. *Front Oncol*. 2018;8:395. https://doi.org/10.3389/fonc.2018.00395
98. Lamba N, Muskens IS, DiRisio AC, et al. Stereotactic radiosurgery versus whole-brain radiotherapy after intracranial metastasis resection: a systematic review and meta-analysis. *Radiat Oncol*. 2017;12(1):106. https://doi.org/10.1186/s13014-017-0840-x
99. Margolin K, Ernstoff MS, Hamid O, et al. Ipilimumab in patients with melanoma and brain metastases: an open-label, phase 2 trial. *Lancet Oncol*. 2012;13(5):459-465. https://doi.org/10.1016/S1470-2045(12)70090-6
100. Kluger HM, Chiang V, Mahajan A, et al. Long-term survival of patients with melanoma with active brain metastases treated with pembrolizumab on a phase II trial. *J Clin Oncol*. 2019;37(1):52-60. https://doi.org/10.1200/JCO.18.00204
101. Long GV, Trefzer U, Davies MA, et al. Dabrafenib in patients with Val600Glu or Val600Lys BRAF-mutant melanoma metastatic to the brain (BREAK-MB): a multicentre, open-label, phase 2 trial. *Lancet Oncol*. 2012;13(11):1087-1095. https://doi.org/10.1016/S1470-2045(12)70431-X
102. Dummer R, Goldinger SM, Turtschi CP, et al. Vemurafenib in patients with *BRAF*^{V600} mutation-positive melanoma with symptomatic brain metastases: final results of an open-label pilot study. *Eur J Cancer*. 2014;50(3):611-621. https://doi.org/10.1016/j.ejca.2013.11.002
103. Welsh SJ, Rizos H, Scolyer RA, Long GV. Resistance to combination BRAF and MEK inhibition in metastatic melanoma: where to next? *Eur J Cancer*. 2016;62:76-85.
104. Vultur A, Villanueva J, Herlyn M. Targeting BRAF in advanced melanoma: a first step toward manageable disease. *Clin Cancer Res*. 2011;17(7):1658-1663. https://doi.org/10.1158/1078-0432.CCR-10-0174
105. U.S. National Library of Medicine. Concurrent Dabrafenib and Trametinib With Sterotactic Radiation in Patients With BRAF Mutation-Positive Malignant Melanoma and Brain Metastases. https://ClinicalTrials.gov/show/NCT02974803. April 9, 2020. Accessed May 28, 2020.
106. U.S. National Library of Medicine. Study to Evaluate Treatment of Dabrafenib Plus Trametinib in Subjects With BRAF Mutation-Positive Melanoma That Has Metastasized to the Brain. https://ClinicalTrials.gov/show/NCT02039947. May 21, 2019. Accessed May 28, 2020.
107. U.S. National Library of Medicine. Vemurafenib and Cobimetinib Combination in BRAF Mutated Melanoma With Brain Metastasis. https://ClinicalTrials.gov/show/NCT02537600. January 27, 2020. Accessed May 28, 2020.

108. U.S. National Library of Medicine. Buparlisib in Melanoma Patients Suffering From Brain Metastases (BUMPER). https://ClinicalTrials.gov/show/NCT02452294. May 3, 2017. Accessed May 28, 2020.
109. U.S. National Library of Medicine. A Study of the Safety and Efficacy of Pembrolizumab (MK-3475) in Combination With Trametinib and Dabrafenib in Participants With Advanced Melanoma (MK-3475-022/KEYNOTE-022). https://ClinicalTrials.gov/show/NCT02130466. March 24, 2020. Accessed May 28, 2020.
110. A Phase 1b Study of Atezolizumab in Combination With Vemurafenib or Vemurafenib Plus Cobimetinib in Participants With BRAFV600-Mutation Positive Metastatic Melanoma. https://ClinicalTrials.gov/show/NCT01656642. May 13, 2020. Accessed May 28, 2020.
111. Ipilimumab With or Without Dabrafenib, Trametinib, and/or Nivolumab in Treating Patients With Melanoma That Is Metastatic or Cannot Be Removed by Surgery. https://ClinicalTrials.gov/show/NCT01940809. May 5, 2020. Accessed May 28, 2020.
112. Silk AW, Bassetti MF, West BT, Tsien CI, Lao CD. Ipilimumab and radiation therapy for melanoma brain metastases. *Cancer Med*. 2013;2(6):899-906.
113. Mathew M, Tam M, Ott PA, et al. Ipilimumab in melanoma with limited brain metastases treated with stereotactic radiosurgery. *Melanoma Res*. 2013;23(3):191-195. https://doi.org/10.1097/CMR.0b013e32835f3d90
114. Knisely JP, James BY, Flanigan J, Sznol M, Kluger HM, Chiang VL. Radiosurgery for melanoma brain metastases in the ipilimumab era and the possibility of longer survival. *J Neurosurg*. 2012;117(2):227-233.
115. Engelman JA, Luo J, Cantley LC. The evolution of phosphatidylinositol 3-kinases as regulators of growth and metabolism. *Nat Rev Genet*. 2006;7(8):606-619. https://doi.org/10.1038/nrg1879
116. Foster FM, Traer CJ, Abraham SM, Fry MJ. The phosphoinositide (PI) 3-kinase family. *J Cell Sci*. 2003;116(15):3037-3040.
117. Hemmings BA, Restuccia DF. PI3K-PKB/Akt pathway. *Cold Spring Harb Perspect Biol*. 2012;4(9):a011189. https://doi.org/10.1101/cshperspect.a011189
118. Yang J, Nie J, Ma X, Wei Y, Peng Y, Wei X. Targeting PI3K in cancer: mechanisms and advances in clinical trials. *Mol Cancer*. 2019;18(1):26. https://doi.org/10.1186/s12943-019-0954-x
119. Kan Z, Jaiswal BS, Stinson J, et al. Diverse somatic mutation patterns and pathway alterations in human cancers. *Nature*. 2010;466(7308):869-873.
120. Meier FE, Forschner A, Garzarolli M, et al. An open-label, uncontrolled, single arm phase II trial of the PI3K inhibitor buparlisib in patients with melanoma brain metastases. *J Clin Oncol*. 2017;35(15 Suppl.):TPS9595. https://doi.org/10.1200/JCO.2017.35.15_suppl.TPS9595
121. Aasen SN, Parajuli H, Hoang T, et al. Effective treatment of metastatic melanoma by combining MAPK and PI3K signaling pathway inhibitors. *Int J Mol Sci*. 2019;20(17):4235. https://doi.org/10.3390/ijms20174235
122. Massard C, Chi KN, Castellano D, et al. Phase Ib dose-finding study of abiraterone acetate plus buparlisib (BKM120) or dactolisib (BEZ235) in patients with castration-resistant prostate cancer. *Eur J Cancer*. 2017;76:36-44.
123. Fazio N, Buzzoni R, Baudin E, et al. A phase II study of BEZ235 in patients with everolimus-resistant, advanced pancreatic neuroendocrine tumours. *Anticancer Res*. 2016;36(2):713-719.
124. De Santis MC, Gulluni F, Campa CC, Martini M, Hirsch E. Targeting PI3K signaling in cancer: Challenges and advances. *Biochim Biophys Acta Rev Cancer*. 2019;1871(2):361-366.
125. Mayer IA, Abramson VG, Formisano L, et al. A phase Ib study of alpelisib (BYL719), a PI3Kα-specific inhibitor, with letrozole in ER+/HER2− metastatic breast cancer. *Clin Cancer Res*. 2017;23(1):26-34.
126. Gopal AK, Kahl BS, de Vos S, et al. PI3Kδ inhibition by idelalisib in patients with relapsed indolent lymphoma. *N Engl J Med*. 2014;370(11):1008-1018. https://doi.org/10.1056/NEJMoa1314583
127. Brosnan EM, Anders CK. Understanding patterns of brain metastasis in breast cancer and designing rational therapeutic strategies. *Ann Transl Med*. 2018;6(9):163.
128. Center for Drug Evaluation and Research. NDA/BLA Multi-disciplinary Review and Evaluation {NDA 212526} {PIQRAY, Alpelisib}. Silver Spring, Maryland: Food and Drug Administration; 2018.

129. U.S. National Library of Medicine. Open-Label Study Evaluating the Safety and Tolerability of LJM716, BYL719 and Trastuzumab in Patients With Metastatic HER2+ Breast Cancer. https://ClinicalTrials.gov/show/NCT02167854. September 17, 2019. Accessed May 28, 2020.
130. U.S. National Library of Medicine. Phosphatidylinositol 3-kinase (PI3K) Alpha iNhibition In Advanced Breast Cancer. https://ClinicalTrials.gov/show/NCT02506556. July 23, 2015. Accessed May 28, 2020.
131. U.S. National Library of Medicine. BYL719 + T-DM1 in HER2(+) Metastatic Breast Cancer Pts Who Progress on Prior Trastuzumab & Taxane Tx. https://ClinicalTrials.gov/show/NCT02038010. March 4, 2020. Accessed May 28, 2020.
132. U.S. National Library of Medicine. Study of the Selective PI3K-Beta Inhibitor GSK2636771 in Combination With Pembrolizumab in Patients With Metastatic Melanoma and PTEN Loss. https://ClinicalTrials.gov/show/NCT03131908. April 13, 2020. Accessed May 28, 2020.
133. Shimoi T, Hamada A, Yamagishi M, et al. PIK3CA mutation profiling in patients with breast cancer, using a highly sensitive detection system. *Cancer Sci*. 2018;109(8):2558-2566. https://doi.org/10.1111/cas.13696
134. Shi H, Hugo W, Kong X, et al. Acquired resistance and clonal evolution in melanoma during BRAF inhibitor therapy. *Cancer Discov*. 2014;4(1):80-93. https://doi.org/10.1158/2159-8290.CD-13-0642
135. Bergholz JS, Roberts TM, Zhao JJ. Isoform-selective phosphatidylinositol 3-kinase inhibition in cancer. *J Clin Oncol*. 2018;36(13):1339-1342. https://doi.org/10.1200/JCO.2017.77.0891
136. Lassen A, Atefi M, Robert L, et al. Effects of AKT inhibitor therapy in response and resistance to BRAF inhibition in melanoma. *Mol Cancer*. 2014;13(1):83. https://doi.org/10.1186/1476-4598-13-83
137. González-Cao M, Rodón J, Karachaliou N, et al. Other targeted drugs in melanoma. *Ann Transl Med*. 2015;3(18):266.
138. Selleck Chemicals. HS-173. https://www.selleckchem.com/products/hs-173.html. Accessed May 28, 2020.
139. Lee H, Jung KH, Jeong Y, Hong S, Hong S-S. HS-173, a novel phosphatidylinositol 3-kinase (PI3K) inhibitor, has anti-tumor activity through promoting apoptosis and inhibiting angiogenesis. *Cancer Lett*. 2013;328(1):152-159. https://doi.org/10.1016/j.canlet.2012.08.020
140. Rumman M, Jung KH, Fang Z, et al. HS-173, a novel PI3K inhibitor suppresses EMT and metastasis in pancreatic cancer. *Oncotarget*. 2016;7(47):78029-78047. https://doi.org/10.18632/oncotarget.12871
141. Kim SJ, Jung KH, Son MK, et al. Tumor vessel normalization by the PI3K inhibitor HS-173 enhances drug delivery. *Cancer Lett*. 2017;403:339-353. https://doi.org/10.1016/j.canlet.2017.06.035
142. Park JH, Jung KH, Kim SJ, et al. Radiosensitization of the PI3K inhibitor HS-173 through reduction of DNA damage repair in pancreatic cancer. *Oncotarget*. 2017;8(68):112893-112906. https://doi.org/10.18632/oncotarget.22850
143. Michmerhuizen NL, Leonard E, Matovina C, et al. Rationale for using irreversible EGFR Inhibitors in combination with PI3K inhibitors for advanced Head and Neck Squamous Cell Carcinoma. *Mol Pharmacol*. 2019;mol-118.
144. Thermo Fisher Scientific. How a Flow Cytometer Works. https://www.thermofisher.com/no/en/home/life-science/cell-analysis/cell-analysis-learning-center/molecular-probes-school-of-fluorescence/flow-cytometry-basics/flow-cytometry-fundamentals/how-flow-cytometer-works.html. Accessed April 3, 2020.
145. Cell Signaling Technology. Overview of Flow Cytometry. https://www.cellsignal.com/contents/_/overview-of-flow-cytometry/flow-cytometry-overview. Accessed April 3, 2020.
146. Bio-Rad Laboratories. Fluorescence Compensation. Flow Cytometry Basics Guide https://www.bio-rad-antibodies.com/flow-cytometry-fluorescence-compensation.html. Accessed April 3, 2020.
147. Molecular Probes, Inc. Alexa Fluor® 488 annexin V/Dead Cell Apoptosis Kit with Alexa® Fluor 488 annexin V and PI for Flow Cytometry. Molecular Probes, Inc.

148. Michmerhuizen NL, Leonard E, Kulkarni A, Brenner JC. Differential compensation mechanisms define resistance to PI3K inhibitors in PIK3CA amplified HNSCC. *Otorhinolaryngol Head Neck Surg*. 2016;1(2):44. https://doi.org/10.15761/OHNS.1000111
149. Lang Q, Ling C. MiR-124 suppresses cell proliferation in hepatocellular carcinoma by targeting PIK3CA. *Biochem Biophys Res Commun*. 2012;426(2):247-252. https://doi.org/10.1016/j.bbrc.2012.08.075
150. Aka JA, Lin SX. Comparison of functional proteomic analyses of human breast cancer cell lines T47D and MCF7. *PLoS ONE*. 2012;7(2):e31532.
151. Bjørnstad OV. *Characterization of Melanoma Brain Metastasis Cell Lines*. Department of Biomedicine, University of Bergen; 2019.
152. Ryoo S-R, Yim Y, Kim Y-K, et al. High-throughput chemical screening to discover new modulators of microRNA expression in living cells by using graphene-based biosensor. *Sci Rep*. 2018;8(1):11413. https://doi.org/10.1038/s41598-018-29633-x
153. Wang X, Ding J, Meng L. PI3K isoform-selective inhibitors: next-generation targeted cancer therapies. *Acta Pharmacol Sin*. 2015;36(10):1170-1176. https://doi.org/10.1038/aps.2015.71
154. Kapałczyńska M, Kolenda T, Przybyła W, et al. 2D and 3D cell cultures - a comparison of different types of cancer cell cultures. *Arch Med Sci*. 2018;14(4):910-919.
155. Moe AM. *The Effect of PARP Inhibitor PJ34 on Metastatic Melanoma Cell Lines*. Department of Biomedicine, University of Bergen; 2016.
156. Sundstrøm T, Prestegarden L, Azuaje F, et al. Inhibition of mitochondrial respiration prevents BRAF-mutant melanoma brain metastasis. *Acta Neuropathol Commun*. 2019;7(1):55. https://doi.org/10.1186/s40478-019-0712-8
157. Häcker G. The morphology of apoptosis. *Cell Tissue Res*. 2000;301(1):5-17.
158. Wallin JJ, Guan J, Edgar KA, et al. Active PI3K pathway causes an invasive phenotype which can be reversed or promoted by blocking the pathway at divergent nodes. *PLoS One*. 2012;7(5):e36402. https://doi.org/10.1371/journal.pone.0036402
159. Dai B, Yan T, Zhang A. ROR2 receptor promotes the migration of osteosarcoma cells in response to Wnt5a. *Cancer Cell Int*. 2017;17(1):112. https://doi.org/10.1186/s12935-017-0482-y
160. Weeraratna AT, Jiang Y, Hostetter G, et al. Wnt5a signaling directly affects cell motility and invasion of metastatic melanoma. *Cancer Cell*. 2002;1(3):279-288. https://doi.org/10.1016/S1535-6108(02)00045-4
161. Dantonio PM, Klein MO, Freire MRV, Araujo CN, Chiacetti AC, Correa RG. Exploring major signaling cascades in melanomagenesis: a rationale route for targetted skin cancer therapy. Biosci Rep. 2018;38(5).
162. Yun S-M, Jung KH, Lee H, et al. Synergistic anticancer activity of HS-173, a novel PI3K inhibitor in combination with Sorafenib against pancreatic cancer cells. *Cancer Lett*. 2013;331(2):250-261. https://doi.org/10.1016/j.canlet.2013.01.007
163. Atkin-Smith GK, Paone S, Zanker DJ, et al. Isolation of cell type-specific apoptotic bodies by fluorescence-activated cell sorting. *Sci Rep*. 2017;7(1):39846. https://doi.org/10.1038/srep39846
164. Jung K, Ryu Y-L, Lee H-S, et al. A novel PI3K inhibitor alleviates fibrotic responses in fibroblasts derived from Peyronie's plaques. *Int J Oncol*. 2013;42(6):2001-2008. https://doi.org/10.3892/ijo.2013.1905
165. Castel P, Scaltriti M. Mechanisms of Resistance to PI3K and AKT Inhibitors. In: Yarden Y, Elkabets M, ed. *Resistance to Anti-Cancer Therapeutics Targeting Receptor Tyrosine Kinases and Downstream Pathways*. Cham, Switzerland: Springer; 2018: 117-146. https://doi.org/10.1007/978-3-319-67932-7_6
166. Luo X-M, Xu B, Zhou M-L, et al. Co-Inhibition of GLUT-1 Expression and the PI3K/Akt signaling pathway to enhance the radiosensitivity of laryngeal carcinoma xenografts *in vivo*. *PLoS One*. 2015;10(11):e0143306. https://doi.org/10.1371/journal.pone.0143306
167. Yamauchi Y, Furukawa K, Hamamura K, Furukawa K. Positive feedback loop between PI3K-Akt-mTORC1 signaling and the lipogenic pathway boosts Akt signaling: induction of the lipogenic pathway by a melanoma antigen. *Cancer Res*. 2011;71(14):4989-4997.
168. Davies MA. The role of the PI3K-AKT pathway in melanoma. *Cancer J*. 2012;18(2):142-147. https://doi.org/10.1097/PPO.0b013e31824d448c

169. Thorsen F, Fite B, Mahakian LM, et al. Multimodal imaging enables early detection and characterization of changes in tumor permeability of brain metastases. J Control Release. 2013;172(3):812-822.
170. Markham A. Alpelisib: first global approval. *Drugs*. 2019;79(11):1249-1253. https://doi.org/10.1007/s40265-019-01161-6